NASA/TM–2014-218303

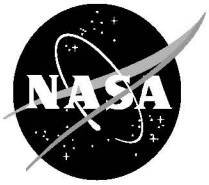

Drought Prediction for Socio-Cultural Stability Project

Christa-Peters Lidard, John B. Eylander, Randall Koster, Balachandrudu Narapusetty, Sujay Kumar, Matt Rodell, John Bolten, David Mocko, Gregory Walker, Kristi Arsenault, Scott Rheingrover

April 2014

NASA STI Program ... in Profile

Since its founding, NASA has been dedicated to the advancement of aeronautics and space science. The NASA scientific and technical information (STI) program plays a key part in helping NASA maintain this important role.

The NASA STI program operates under the auspices of the Agency Chief Information Officer. It collects, organizes, provides for archiving, and disseminates NASA's STI. The NASA STI program provides access to the NASA Aeronautics and Space Database and its public interface, the NASA Technical Report Server, thus providing one of the largest collections of aeronautical and space science STI in the world. Results are published in both non-NASA channels and by NASA in the NASA STI Report Series, which includes the following report types:

- TECHNICAL PUBLICATION. Reports of completed research or a major significant phase of research that present the results of NASA Programs and include extensive data or theoretical analysis. Includes compilations of significant scientific and technical data and information deemed to be of continuing reference value. NASA counterpart of peer-reviewed formal professional papers but has less stringent limitations on manuscript length and extent of graphic presentations.
- TECHNICAL MEMORANDUM. Scientific and technical findings that are preliminary or of specialized interest, e.g., quick release reports, working papers, and bibliographies that contain minimal annotation. Does not contain extensive analysis.
- CONTRACTOR REPORT. Scientific and technical findings by NASA-sponsored contractors and grantees.
- CONFERENCE PUBLICATION. Collected papers from scientific and technical conferences, symposia, seminars, or other meetings sponsored or co-sponsored by NASA.
- SPECIAL PUBLICATION. Scientific, technical, or historical information from NASA programs, projects, and missions, often concerned with subjects having substantial public interest.
- TECHNICAL TRANSLATION. English-language translations of foreign scientific and technical material pertinent to NASA's mission.

Specialized services also include organizing and publishing research results, distributing specialized research announcements and feeds, providing help desk and personal search support, and enabling data exchange services. For more information about the NASA STI program, see the following:

- Access the NASA STI program home page at http://www.sti.nasa.gov
- E-mail your question via the Internet to help@sti.nasa.gov
- Fax your question to the NASA STI Help Desk at 443-757-5803
- Phone the NASA STI Help Desk at 443-757-5802
- Write to:

  NASA STI Help Desk
  NASA Center for AeroSpace Information
  7115 Standard Drive
  Hanover, MD 21076-1320

Available from:

NASA Center for AeroSpace Information
7115 Standard Drive
Hanover, MD 21076-1320

National Technical Information Service
5285 Port Royal Road
Springfield, VA 22161

NASA/TM–2014-218303

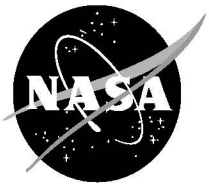

Drought Prediction for Socio-Cultural Stability Project

Christa-Peters Lidard
Goddard Space Flight Center, Greenbelt, MD

John B. Eylander
U. S. Army ERDC/CRREL, Hanover, NH

Randall Koster
Goddard Space Flight Center, Greenbelt, MD

Balachandrudu Narapusetty
Science Applications International Corporation, McLean, VA

Sujay Kumar
Science Applications International Corporation, McLean, VA

Matt Rodell
Goddard Space Flight Center, Greenbelt, MD

John Bolten
Goddard Space Flight Center, Greenbelt, MD

David Mocko
Science Applications International Corporation, McLean, VA

Gregory Walker
Science Applications International Corporation, McLean, VA

Kristi Arsenault
Science Applications International Corporation, McLean, VA

Scott Rheingrover
Science Applications International Corporation, McLean, VA

National Aeronautics and
Space Administration

Goddard Space Flight Center
Greenbelt, MD

April 2014

Level of Review: This material has been technically reviewed by technical management

Abstract

The primary objective of this project is to answer the question: "Can existing, linked infrastructures be used to predict the onset of drought months in advance?" Based on our work, the answer to this question is "yes" with the qualifiers that skill depends on both lead-time and location, and especially with the associated teleconnections (e.g., ENSO, Indian Ocean Dipole) active in a given region/season.

As part of this work, we successfully developed a prototype drought early warning system based on existing/mature NASA Earth science components including the Goddard Earth Observing System Data Assimilation System Version 5 (GEOS-5) forecasting model, the Land Information System (LIS) land data assimilation software framework, the Catchment Land Surface Model (CLSM), remotely sensed terrestrial water storage from the Gravity Recovery and Climate Experiment (GRACE) and remotely sensed soil moisture products from the Aqua/Advanced Microwave Scanning Radiometer – EOS (AMSR-E). We focused on a single drought year—2011—during which major agricultural droughts occurred with devastating impacts in the Texas-Mexico region of North America (TEXMEX) and the Horn of Africa (HOA).

Our results demonstrate that GEOS-5 precipitation forecasts show skill globally at 1-month lead, and can show up to 3 months skill regionally in the TEXMEX and HOA areas. Our results also demonstrate that the CLSM soil moisture percentiles are a good indicator of drought, as compared to the North American Drought Monitor for TEXMEX and a combination of Famine Early Warning Systems Network (FEWS NET) data and Moderate Resolution Imaging Spectroradiometer (MODIS)'s Normalized Difference Vegetation Index (NDVI) anomalies over HOA.

The data assimilation experiments produced mixed results. GRACE terrestrial water storage (TWS) assimilation was found to significantly improve soil moisture and evapotranspiration, as well as drought monitoring via soil moisture percentiles, while AMSR-E soil moisture assimilation produced marginal benefits.

We carried out 1-3 month lead-time forecast experiments using GEOS-5 forecasts as input to LIS/CLSM. Based on these forecast experiments, we find that the expected skill in GEOS-5 forecasts from 1-3 months is present in the soil moisture percentiles used to indicate drought. In the case of the HOA drought, the failure of the long rains in April appears in the February 1, March 1 and April 1 initialized forecasts, suggesting that for this case, drought forecasting would have provided some advance warning about the drought conditions observed in 2011.

Three key recommendations for follow-up work include: (1) carry out a comprehensive analysis of droughts observed over the entire period of record for GEOS-5 forecasts; (2) continue to analyze the GEOS-5 forecasts in HOA stratifying by anomalies in long and short rains; and (3) continue to include GRACE TWS, Soil Moisture/Ocean Salinity (SMOS) and the upcoming NASA Soil Moisture Active/Passive (SMAP) soil moisture products in a routine activity building on this prototype to further quantify the benefits for drought assessment and prediction.

Table of Contents

List of Figures

List of Tables

I. BACKGROUND

A. Objective

The primary objective was to address the question: "Can existing, linked infrastructures be used to predict the onset of drought months in advance?" by developing a prototype drought early warning system based on existing/mature NASA Earth science.

B. Approach

Building on previous work demonstrating that drought early warning skill is a mixture of forecast skill and land state memory and initial conditions, the rationale for the work was to construct a system capable of harnessing all available skill from GEOS-5 seasonal forecasts and land state initialization via assimilation of AMSR-E and GRACE through LIS. Our approach consisted of 5 tasks that not only connect the components for a prototype global drought early warning system, but evaluate the products of the system for the 2011 droughts in Texas and the Horn of Africa. The tasks include 1) evaluating GEOS-5 forecast skill for 2011; 2) conducting a long-term (1948-2011) offline spinup with the LIS/Catchment model using observed forcing; 3) conducting additional spinups from 2008-forward with AMSR-E and GRACE assimilation; 4) conducting forecast experiments using GEOS-5 using the spinups with and without AMSR-E and GRACE DA initial land states; and 5) evaluating the skill of the forecasted droughts.

C. Description of GEOS-5 Model, MERRA and MERRA-Land

The Global Modeling and Assimilation Office (GMAO) at NASA/GSFC hosts a seasonal forecast system consisting of an atmospheric general circulation model (AGCM, Rienecker *et al.* 2008) coupled to the Catchment land surface model (Koster et al. 2000) and a full ocean GCM imported from the NOAA Geophysical Fluid Dynamics Laboratory (Griffies *et al.* 2005). The Goddard Earth Observing System Model, Version 5 (GEOS-5) is a system of models integrated using the Earth System Modeling Framework (ESMF). The GEOS-5 Data Assimilation System integrates the GEOS-5 AGCM with the Gridpoint Statistical Interpolation (GSI) atmospheric analysis developed jointly with NOAA/NCEP/EMC. The GEOS-5 systems are being developed in the GMAO to support NASA's earth science research in data analysis, observing system modeling and design, climate and weather prediction, and basic research. As part of GMAO quasi-operational activities, the atmosphere, land, and ocean states of the coupled models are initialized each month to realistic values, and (by varying the start date) an ensemble of 9-month simulations generates the forecasts of meteorological forcing, particularly precipitation, that are used in this project. The hourly forecasts are available from 1980-present, at a spatial resolution of 1.25 degrees latitude x 1 degree longitude. The experimental forecasts and historical performance can be viewed at the Experimental Climate Forecast web page (http://gmao.gsfc.nasa.gov/cgi-bin/products/climateforecasts/GEOS5/index.cgi). See http://gmao.gsfc.nasa.gov/research/climate/ for more information on the forecast system.

The Modern-Era Retrospective Analysis for Research and Applications (MERRA) is a NASA reanalysis for the satellite era that utilizes a fixed version of the Goddard Earth Observing System Data Assimilation System Version 5 (GEOS-5). The MERRA time period covers the modern era of remotely sensed data, from 1979 through the present, and the special focus of the atmospheric assimilation is the hydrological cycle. Previous long-term reanalyses of the Earth's climate had high levels of uncertainty in precipitation and in precipitation's interannual variability. The GEOS-5 data assimilation system used for MERRA implements Incremental Analysis Updates (IAU) to slowly adjust the model states toward the observed state. The water cycle benefits as unrealistic spin down is minimized. In addition, the model physical parameterizations have been tested and evaluated in a data assimilation context, which also reduces the shock of adjusting the model system. Land surface processes are modeled with the state-of-the-art GEOS-5 Catchment hydrology land surface model (described below). MERRA thus makes significant advances in the representation of the water cycle in reanalyses.

MERRA output data resemble other global reanalyses, with several key advances, including output at frequencies higher than the 6-hourly analyses. Two-dimensional diagnostics (surface fluxes, single level meteorology, vertical integrals and land states) are produced at 1-hour intervals. These data products and the 6-hourly three-dimensional atmospheric analyses are also available at the full spatial resolution (1/2 degrees latitude × 2/3 degrees longitude). Extensive three-dimensional 3-hourly atmospheric diagnostics on 42 pressure levels are also available, but at coarser (1.25 degree) resolution.

An improved set of land surface hydrological fields is provided in the supplemental MERRA-Land data product. In addition to the above-mentioned improvements, this product benefits from NOAA Climate Prediction Center observation-based corrections to the precipitation forcing and from revised parameter values in the rainfall interception model, changes that effectively correct for known limitations in the MERRA surface meteorological forcings. The MERRA-Land products are documented by Reichle et al. (2011) and Reichle (2012), who found that the MERRA-Land data appear more accurate than the original MERRA estimates and are thus recommended for those interested in using MERRA output for land surface hydrological studies. Like MERRA, MERRA-Land analyses are available hourly on a grid with the same spatial resolution (1/2 degrees latitude × 2/3 degrees longitude).

D. Description of Catchment Land Surface Model

The land surface model being used in this project is the Catchment Land Surface Model (CLSM; Koster et al., 2000; Ducharne et al., 2000), which calculates the water and energy balance of the land surface using either observed or forecasted inputs such as precipitation, radiation, wind speed, temperature, humidity and pressure. For this work, we utilize the Fortuna 2.5 version of Catchment, which is the version used operationally in GEOS-5.7.2 since Aug 2011, and also in MERRA-Land.

Unlike most LSMs, CLSM does not employ a one-dimensional "layered" framework, using instead a framework that emphasizes subgrid spatial variability in moisture. In this LSM, subgrid heterogeneity in surface moisture state is treated statistically, since computational constraints (now and in the foreseeable future) prevent its explicit resolution. Nevertheless, the applied distributions are related sensibly to the topography, which exerts a major control over much of the subgrid variability. The approach is illustrated in Figure B.1 which shows three different levels of the (shallow) water table and the associated partitioning of the surface into three regions: (1) a saturated region, from which evaporation occurs with no water stress and over which rainfall is immediately converted to surface runoff, (2) a subsaturated region, from which transpiration occurs with limited water stress and over which rainwater infiltrates the soil, and (3) a "wilting" region, in which the water stress shuts down the transpiration completely. The relative areas of these regions, which vary in time, are unique functions of the local topography and the values of the Catchment LSM's three water prognostic variables. By continually partitioning the catchment into hydrologically distinct regimes and then applying different runoff and evaporation physics in the different regimes, the Catchment LSM should, at least in principle, produce a more realistic simulation of area-averaged surface energy and water processes.

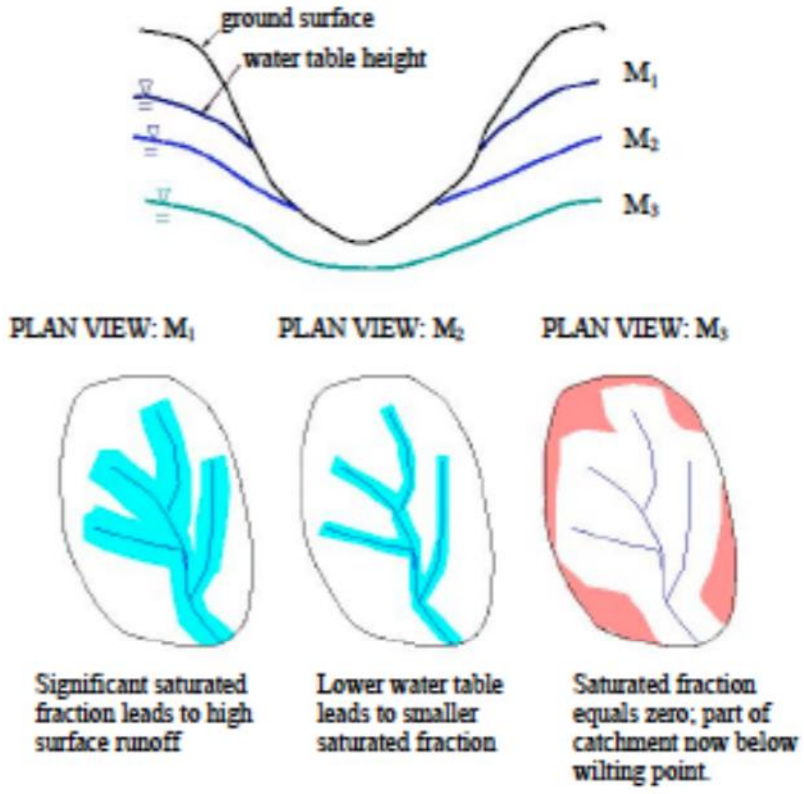

Figure 1. Separation of the catchment area into hydrological regimes.

The soil water prognostic variables used by the Catchment LSM are "non-traditional" in that they are not strictly associated with soil layers. The main variable, the "catchment deficit", describes the equilibrium water table distribution and the associated distribution of the equilibrium soil moisture profiles in the overlying vadose zone. The second variable describes the degree to which the root zone is out of equilibrium with the catchment deficit, and the third describes the degree to which the near-surface moisture is out of equilibrium with the other two variables. The water transfer between the three variables and the baseflow flux out of the system are controlled in part by the local topography.

The model's other prognostic variables include an interception reservoir water content, a surface temperature, and the heat contents of six subsurface soil layers, from which time-varying vertical profiles of soil temperature over several meters can be derived. The model allows explicit vegetation control over the computed surface energy and water balances, with environmental stresses (high temperatures, dry soil, etc.) acting to increase canopy resistance and thus decrease transpiration. Six fundamentally different types of vegetation are considered in the current version of the Catchment LSM: broadleaf evergreen trees, broadleaf deciduous trees, needleleaf trees, grassland, shrubs, and tundra vegetation. Bare soil evaporation, transpiration, and interception loss occur in parallel. The energy balance formulations in the model (again, applied separately in each hydrological regime) were derived in large part from the Mosaic land surface model (Koster and Suarez, 1996), which in turn borrowed heavily from the SiB model of Sellers et al. (1986) for the transpiration calculation. Snow is modeled using three prognostic variables (heat content, snow water equivalent, and snow depth) in each of three layers (Stieglitz et al., 2001). The melting and refreezing of snow, snow compaction, liquid water retention, and the impact of snow density on thermal conductivity and albedo are explicitly treated.

E. Description of Land Information System

NASA/GSFC has led the development of a comprehensive land surface modeling and data assimilation framework known as the NASA Land Information System (LIS; Kumar et al. 2006, Peters-Lidard et al. 2007). LIS provides the modeling and computational capabilities to merge observations and model forecasts to generate spatially and temporally coherent estimates of land surface conditions. These analyses are of critical importance to applications such as agricultural production, water resources management, and prediction of flood, drought, weather and climate.

LIS includes a comprehensive suite of subsystems to support uncoupled and coupled land data assimilation, as shown in Figure 2. The LIS-LSM subsystem includes several community land surface models (LSMs), such as the CLSM described above, and supports their application at varying spatial and temporal scales, over regional, continental and global domains.

The LIS Data Assimilation (LIS-DA; Kumar et al., 2008) subsystem supports multiple data assimilation algorithms that are focused on generating improved estimates of hydrologic model

states. The LIS-DA subsystem includes tools such as the Ensemble Kalman Filter (EnKF), which is widely accepted as an effective technique for sequential assimilation of hydrologic variables. The EnKF provides a flexible approach for incorporating errors in the model and observations and its ensemble-based treatment of errors makes it suitable for handling the modestly non-linear dynamics and the temporal discontinuities that are typical of land surface processes. The LIS-DA subsystem is uniquely suited for assimilating disparate sources of observations into different land surface models. Retrievals of soil moisture from AMSR-E (Kumar et al., 2009; Peters-Lidard et al., 2011), skin temperature from ISCCP (Reichle et al., 2009), and snow water equivalent and snow cover from AMSR-E and MODIS (Yatheendradas, et al., 2012; Liu et al., 2013) have been assimilated into land surface models using LIS-DA. In addition, recently funded work will extend LIS-DA to allow direct radiance assimilation to overcome the limitations of the retrieval products.

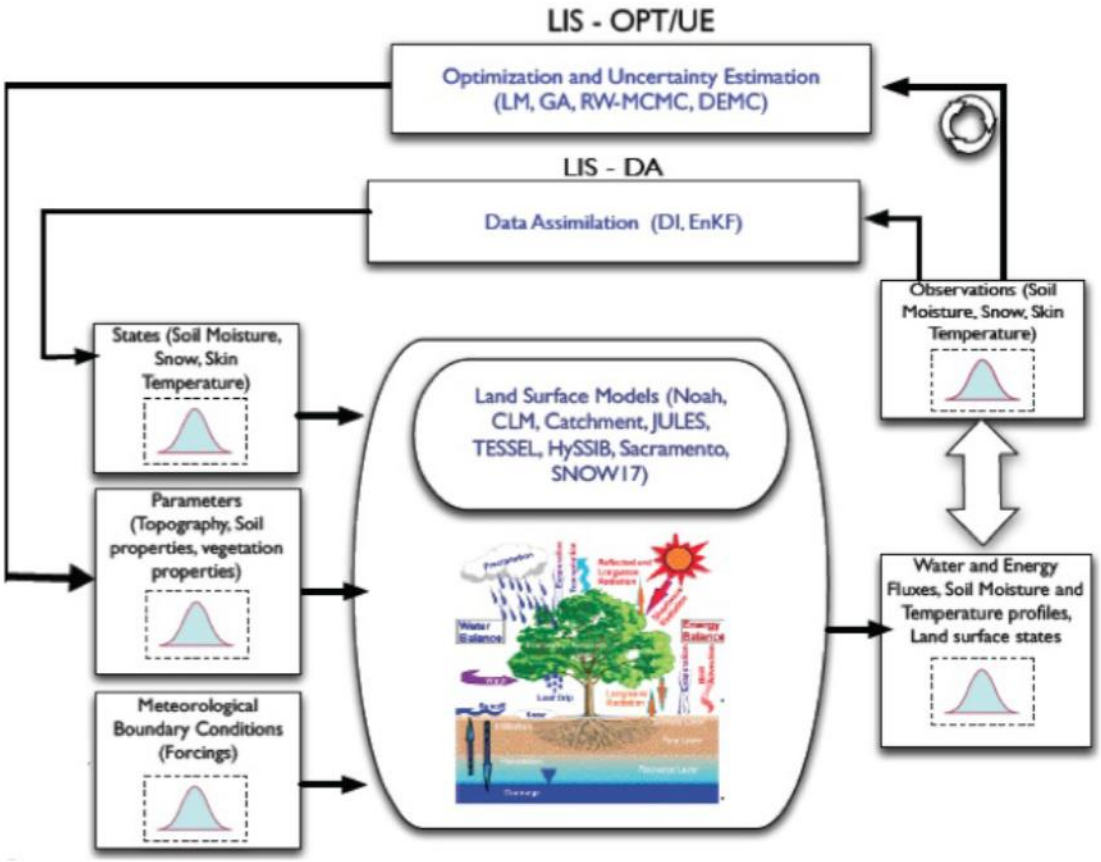

Figure 2. Schematic of LIS showing the three subsystems of LIS described in the text, LIS-LSM, LIS-DA and LIS-OPT/UE.

The newest version of LIS (version 7 or LIS7), which is the version used for this project, includes a suite of subsystems for optimization (LIS-OPT) and uncertainty estimation (LIS-UE). These subsystems were demonstrated for satellite OSSEs related to soil moisture estimation

(Kumar et al. 2012a). Through the uncertainty estimation tools, the remotely sensed observations were used to quantify the uncertainty in model parameters and model predictions (Harrison et al. 2012). Overall, the integrated modeling, multi-scale resolution, ensemble run capabilities, inclusion of algorithms for exploiting space-based observations, and verification capabilities uniquely position LIS to serve as a platform for data assimilation experiments, including those used in this project.

LIS7 utilizes a standard preprocessing toolkit known as the Land Data Toolkit (LDT) and relies heavily on an open-source post-processing analysis software package (Land surface Verification Toolkit (LVT); Kumar et al. 2012b).

II. TECHNICAL ACCOMPLISHMENTS

A. GEOS-5 Forecast Skill

The underlying premise of this work is that early warning skill for agricultural drought (deficits in soil moisture) is a mixture of meteorological forecast skill and land state memory combined with accurate initial conditions. To evaluate meteorological forecast skill for drought early warning applications, the most important forecast variable is precipitation. Hence, this section summarizes our findings with respect to GEOS-5 precipitation forecast skill for the HOA and TEXMEX domains.

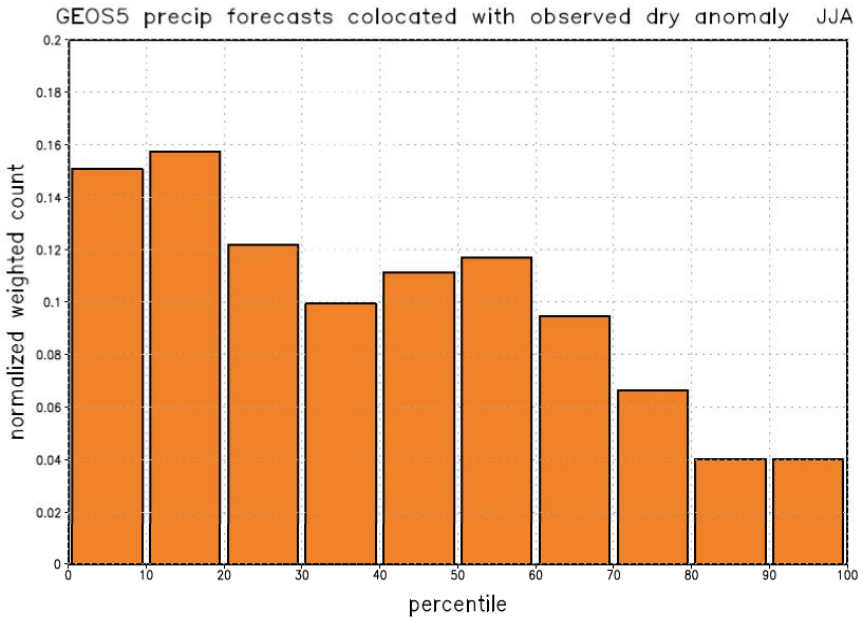

Figure 3. Histogram showing the decile of forecasted JJA precipitation (i.e., 0-10 = driest decile) for those locations and times when the observed JJA precipitation is in its lowest decile. To avoid noise associated with uncertain precipitation observations, a weighting defined by precipitation gauge density is applied to the data prior to binning.

First, though, we provide in Figure 3 a global look at how well the GEOS-5 system predicts precipitation deficits. The histogram, which shows data for 3-month (June-August, or JJA) precipitation forecasts at zero lead covering the period 1981-2012, was constructed as follows.

Thirty-two years of NOAA PREC/L precipitation observations were analyzed at a resolution of 5°×5°, and at each location, years for which the JJA precipitation lay in the lowest decile of observed values at that location were determined. We then examined the ensemble mean forecasts of JJA precipitation. We determined, for each instance of low observed JJA precipitation, the decile in which the corresponding forecasted precipitation fell. The histogram shows the distribution of these deciles. A perfect model performance would put all the counts in the first (0-10) decile; as can be seen, the forecasting system is far from perfect. (Seasonal precipitation prediction is a notoriously difficult and universal problem. Skill with our system for temperature prediction, not shown, is significantly higher.) There is nevertheless some tendency for the model to predict drier-than-average conditions when it is supposed to; this is the information we want to exploit in this project.

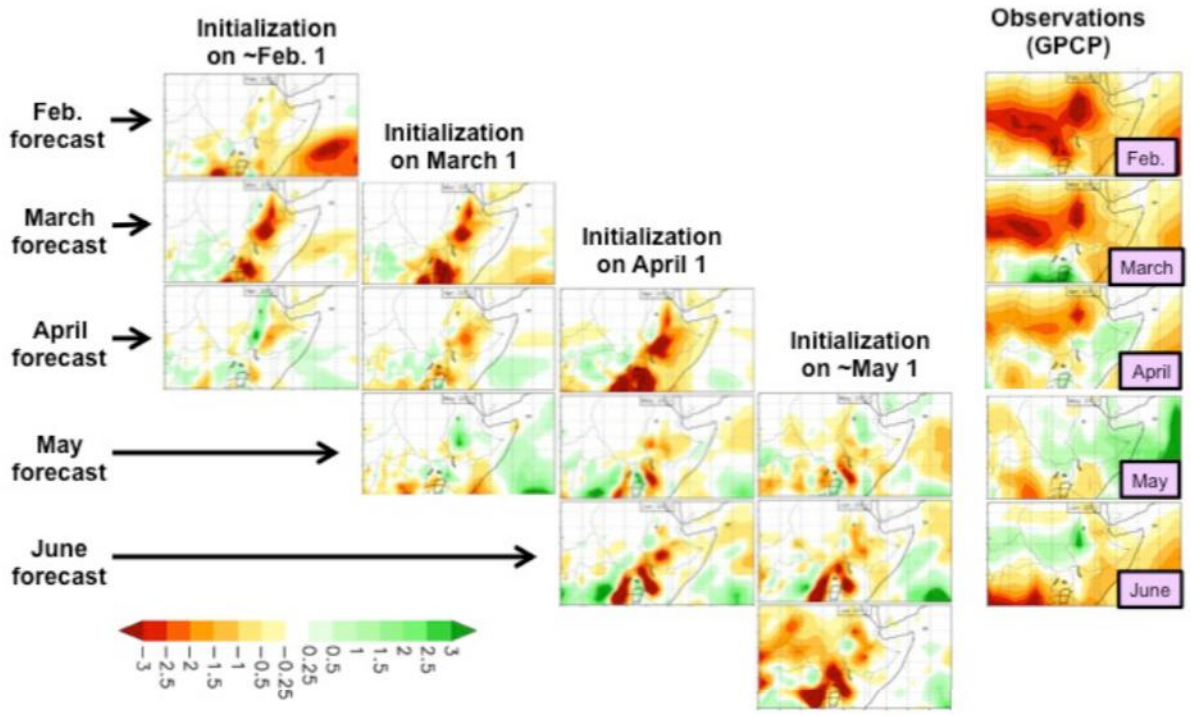

Figure 4. Monthly ensemble mean GEOS-5 precipitation anomaly forecasts over the Horn of Africa for different initialization dates and lead times. Observed anomalies appear in the rightmost column.

The skill of the GEOS-5 system in predicting the 2011 Texas drought is discussed in an online GMAO report (http://gmao.gsfc.nasa.gov/research/climate/US_drought/); in short, predicted dry conditions tend to be displaced eastward from Texas, though the Texas heat wave itself is reasonably well predicted. A corresponding analysis of the system's performance in predicting the 2011 Horn of Africa drought is provided in Figure 4. The model shows some slight skill in predicting this drought – at least some of its large-scale features if not the specific details of its structure – even at 1-month lead (for the February 1 initialization). The forecasted drought, however, is generally much less severe than the actual drought. This, of course, may represent

deficiencies in the forecast system. It must certainly also reflect, however, the unavoidable fact that the forecast results represent an ensemble average, whereas the observations represent a single "realization" of weather – plots for some of the individual ensemble members will look much more realistic. Differences may also reflect deficiencies in the observational record over the area.

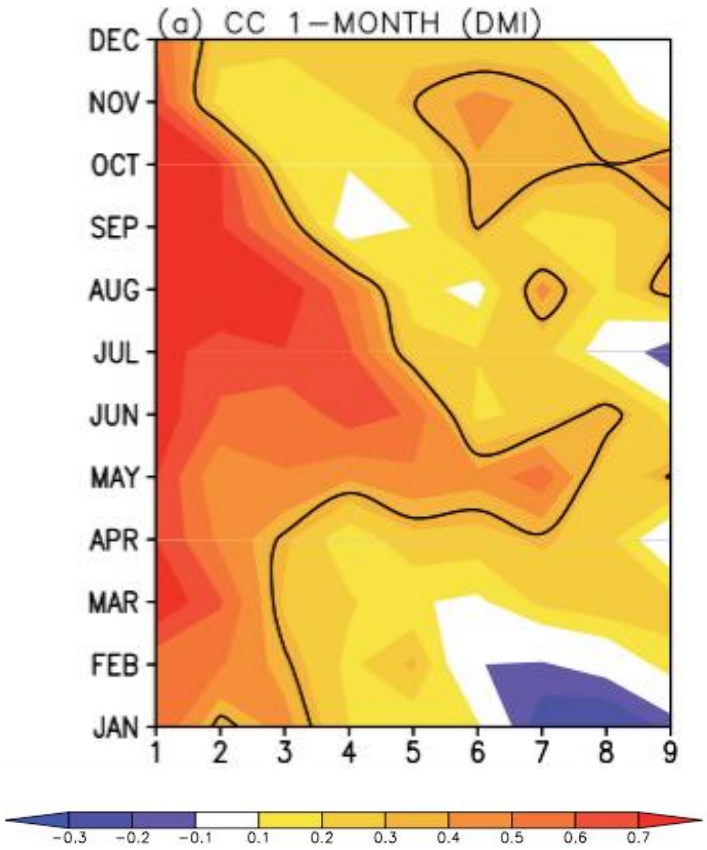

Figure 5. Correlation coefficients between the observed and GEOS-5 forecasted Dipole Mode Index (DMI) at different lead times and for different starting months. The DMI is defined as the difference in Sea Surface Temperature (SST) anomalies between (i) 50°-70°E; 10°S-10°N and (ii) 90°-110°E; 10°S-Eq). 5% significant correlations are shown by the solid black lines.

Recent work (Behera et al., 2005; Saji et al., 1999) suggests that the Indian Ocean Dipole exhibits a strong control on the precipitation in the HOA region. Behera et al., found significant correlation with the short rains (Oct-Nov) and Saji et al., found correlation with the long rains (Apr-May). To investigate whether the GEOS-5 model captures this sea surface temperature anomaly, we first examined the ability of the model to forecast the Dipole Mode Index (DMI) at different lead times and starting months (Figure 5). As this figure shows, the GEOS-5 model

successfully forecasts this feature at lead times of 2-3 months and often much more than 3 months for start months of May through September.

To further quantify the skill of GEOS-5 in representing this teleconnection, we examine the correlation coefficients between GEOS-5 forecasted and observed 1- and 2-month aggregated precipitation anomalies over HOA for 1981-2012. As shown in Figure 6, the skill for the long rain months is generally small, but the skill for the short rain months ranges from 2-3 months.

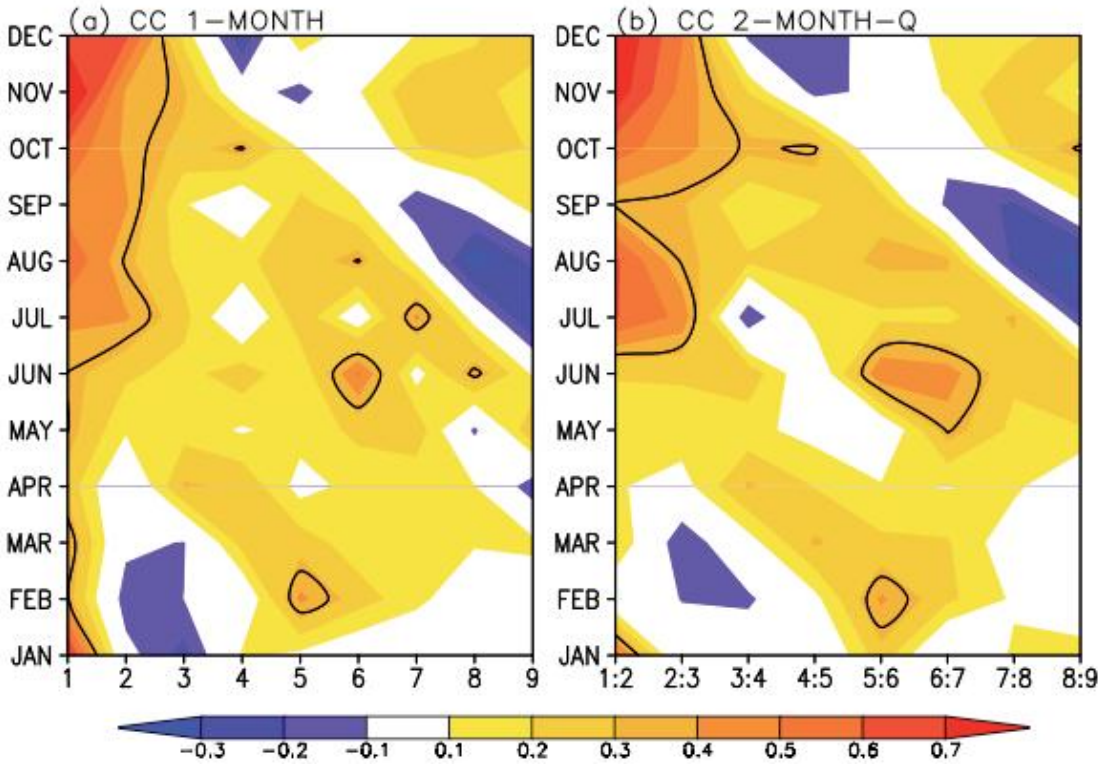

Figure 6. Correlation coefficients between GEOS-5 forecasted and observed 1- and 2-month aggregated precipitation anomalies over HOA for 1981-2012. 5% significant correlations are shown with a solid black line.

Finally, the probabilistic skill of the forecasts is evaluated using reliability diagrams (Wilks 1995). Reliability diagrams explain a model's ability to forecast extreme events based on the probability in capturing an observed extreme event among the model ensembles. The information provided by reliability diagrams is two-fold. First, it reveals the probability that a group of model ensembles forecast a particular event, and secondly, the probability obtained by the first step is compared against the observational occurrence of the event to understand the forecast reliability. The synthesis of these two steps provides a basis for the probabilistic verification skill in the reliability diagrams. The reliability diagrams can be studied on gridded data (Barnston et al. 2003) as well as on area specific indices such as Niño 3.4 (Saha et al. 2006).

For the Horn of Africa (HOA) case shown in Figure 7, reliability diagrams are constructed for 1-month lead forecasts obtained from each grid point. The reliability of the forecasts is studied optimally based on five forecast probability bins falling in the 0-1/7, 1/7-2/7, 2/7-3/7, 3/7-4/7, 4/7-5/7, 5/7-6/7, 6/7-7/7, and 1 probability categories. Figures 7a and 7b show the model forecasts' reliability in reproducing lowest decile and lower half of the precipitation, respectively. In each of the subplots of figure 7, the right-side column of histograms show the number of samples that fall into the probability bins for summer (J-J-A), fall (S-O-N), winter (D-J-F) and spring (M-A-M) seasons.

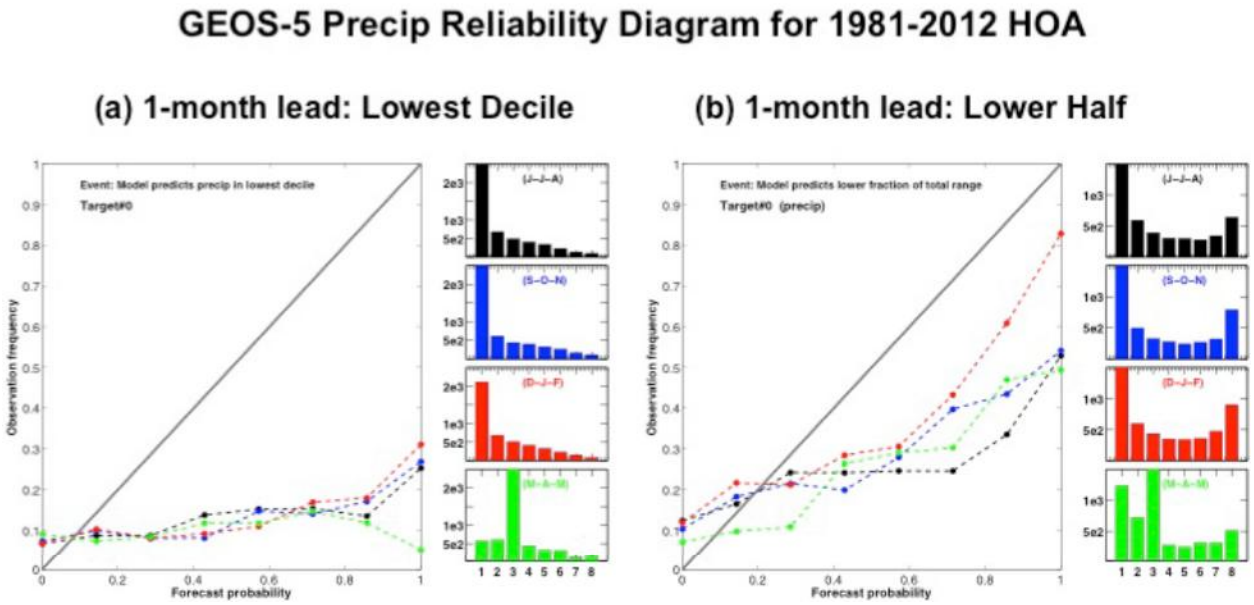

Figure 7. Reliability diagram for (a) lowest decile and (b) lower half of the GEOS-5 1-month lead precipitation forecasts over HOA.

In our reliability diagrams, the condition for the forecast probability versus observation frequency is that the GEOS5 precipitation forecasts are falling in the lowest decile concurrent with observations following the same. The grey diagonal line in all the plots indicates that model forecasts predict exactly the observed event, and should be considered as a reference for perfect reliability. Curves above the perfect reliability indicate that the model gives false alarms, where as curves located below denote that the model underpredicts the events. Generally, a flat reliability curve compared to the ideal-scenario grey line indicates over-confident and persistent nature of forecasts (Barnston et al. 2003). The GEOS5 ensemble forecasts generally over-predicted the lowest decile of the precipitation compared to observations (figure 7a), however, the lower half of the precipitations are more closely reproduced with respect to observations (figure 7b).

B. Long-term LIS/CLSM Spinups and Open Loop

As described above, CLSM is embedded in the LIS framework to create "hindcasts", which are retrospective simulated forecasts, of hydrological conditions related to drought. Two domains

that experienced drought in 2011 are considered in this work: the Horn of Africa (HOA: 21.25°E-51.25°E; 11.25°S-23.75°N) and TEXas-MEXico (TEXMEX: 111.25°W-86.25°W; 18.75°N-41.25°N) regions, as shown in Figure 8.

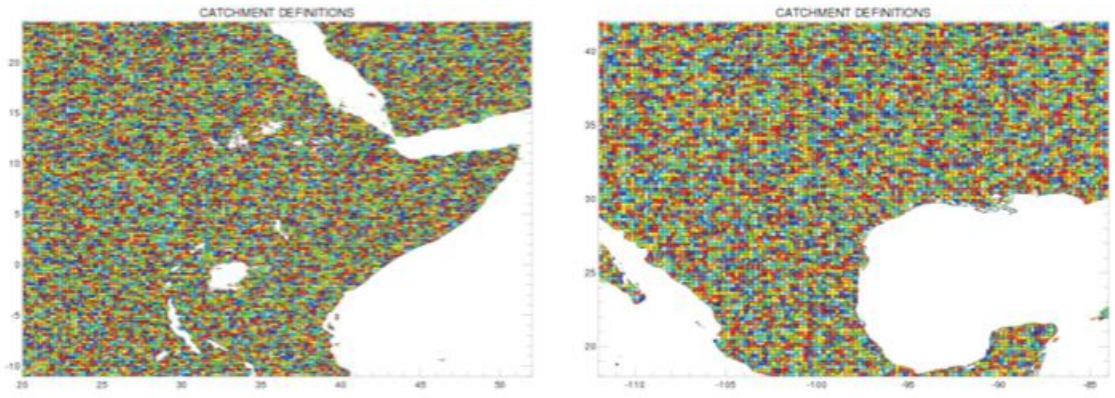

Figure 8. CLSM Catchments for the HOA (left) and TEXMEX (right) domains.

However, in order to initialize these hindcasts, the land surface model must first be run for a long-term period in order for slowly evolving land surface states such as soil moisture profiles and water table depths to reach equilibrium conditions that are suitable for use in simulated forecast experiments. The process of running a land surface model for a long period of time using observed precipitation inputs is known as "spinup", and requirements and recommended methodologies for spinup have been discussed by Cosgrove et al., (2003) and Rodell et al., (2005), among others.

For this project, we utilized the same spinup methodology as MERRA-Land. First, we conduct two 31-year spinups (1980-2011) using the MERRA-Land meteorological data as inputs or "forcings" for LIS/CLSM; the system is restarted on 1 January 1980 when the end of 31 December 2011 is reached, using the 31 December 2011 land states. Once the 62-year spinup is complete, we run a final 31-year "open loop" run starting 1 January 1980, where the term "open loop" refers to a LIS/CLSM run after spinup and without any data assimilation. This "open loop" run is used to establish the LIS/CLSM climatology that is used both for data assimilation and for calculation of drought-related indices.

Below, we describe the experimental setup for the spinup and open loop runs for both the HOA and TEX-MEX domains.

1. Experiment Setup

The horizontal spatial grids for the Horn of Africa and TEXas-MEXico domains are both 0.25°, which roughly correspond to the 25km resolution of the remotely sensed soil moisture data. In

addition to the catchments shown in Figure 9, the experiment setup requires soil, land cover/vegetation and geological parameters.

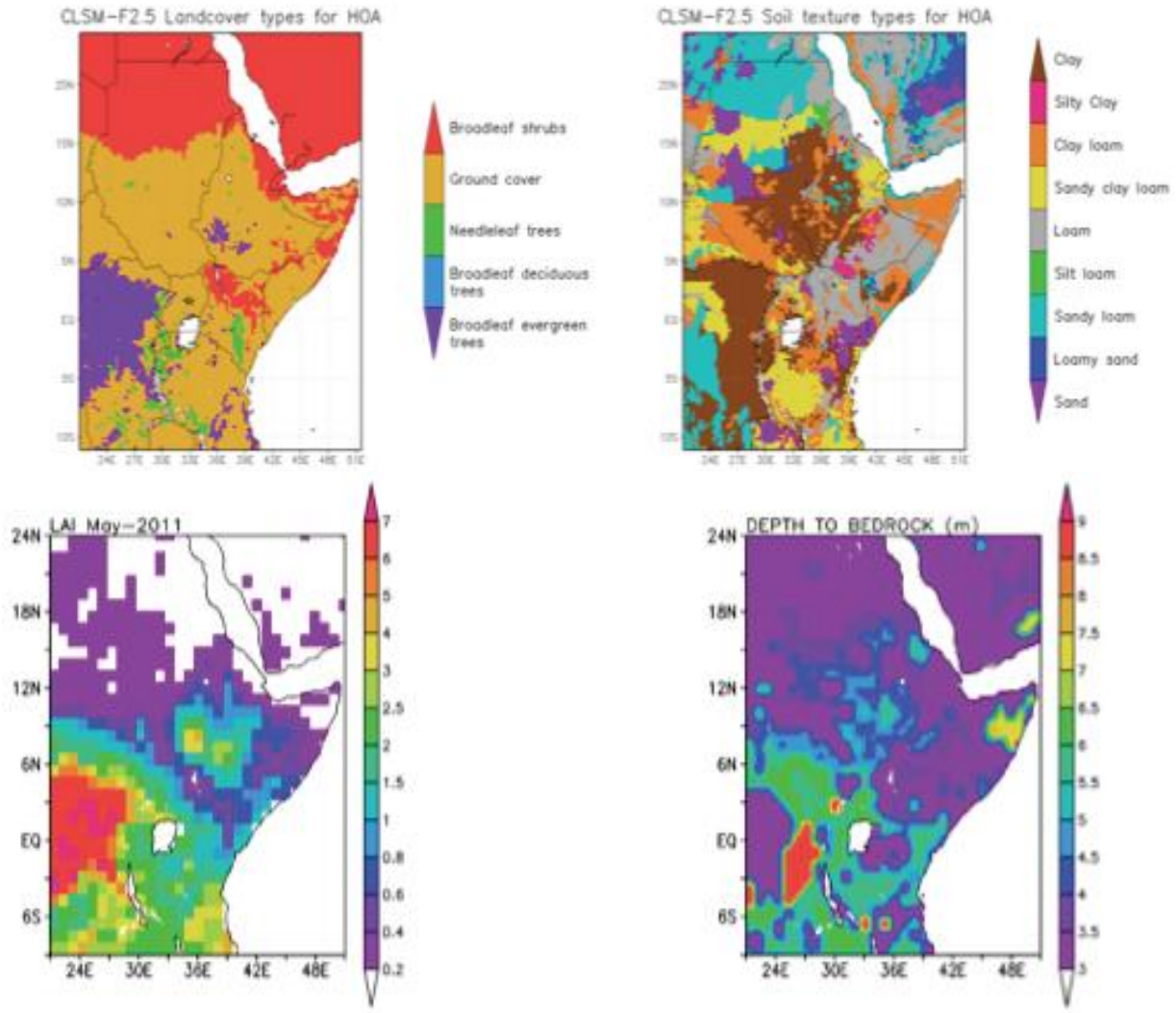

Figure 9. Land cover type, soil type, May Leaf Area Index, and depth to bedrock for the HOA domain.

In the case of the HOA domain, these input parameters are shown in Figure 9, and Figure 10 shows these parameters for TEXMEX. The CLSM parameters for the Fortuna2.5 version used in MERRA-Land are described in Reichle et al., (2012), and include the following sources:

- Topography: GTOPO30.
- Soils: NGDC soil textures at 1/12th-degree by 1/12th-degree.
- Landcover: IGBP classified using SiB-2 land cover classification data at 1-min.
- LAI: AVHRR climatology developed for GSWP-2 at 1-degree, monthly.
- Depth to bedrock: GSWP-2 data at 1-degree.

Based on recent work over the region by co-Is Rodell and Bolten, the depth to bedrock in our simulations is set approximately 2m deeper compared to that in MERRA-Land. This allows the water table to properly evolve and incorporate GRACE data without hitting unrealistic bounds during extreme wet or dry events, such as the 2011 drought. Due to the change in bedrock depth along with the difference in spatial resolution for the LIS/CLSM runs relative to MERRA-Land, a completely new CLSM parameter set was derived for this work using the GMAO preprocessor for CLSM-Fortuna 2.5.

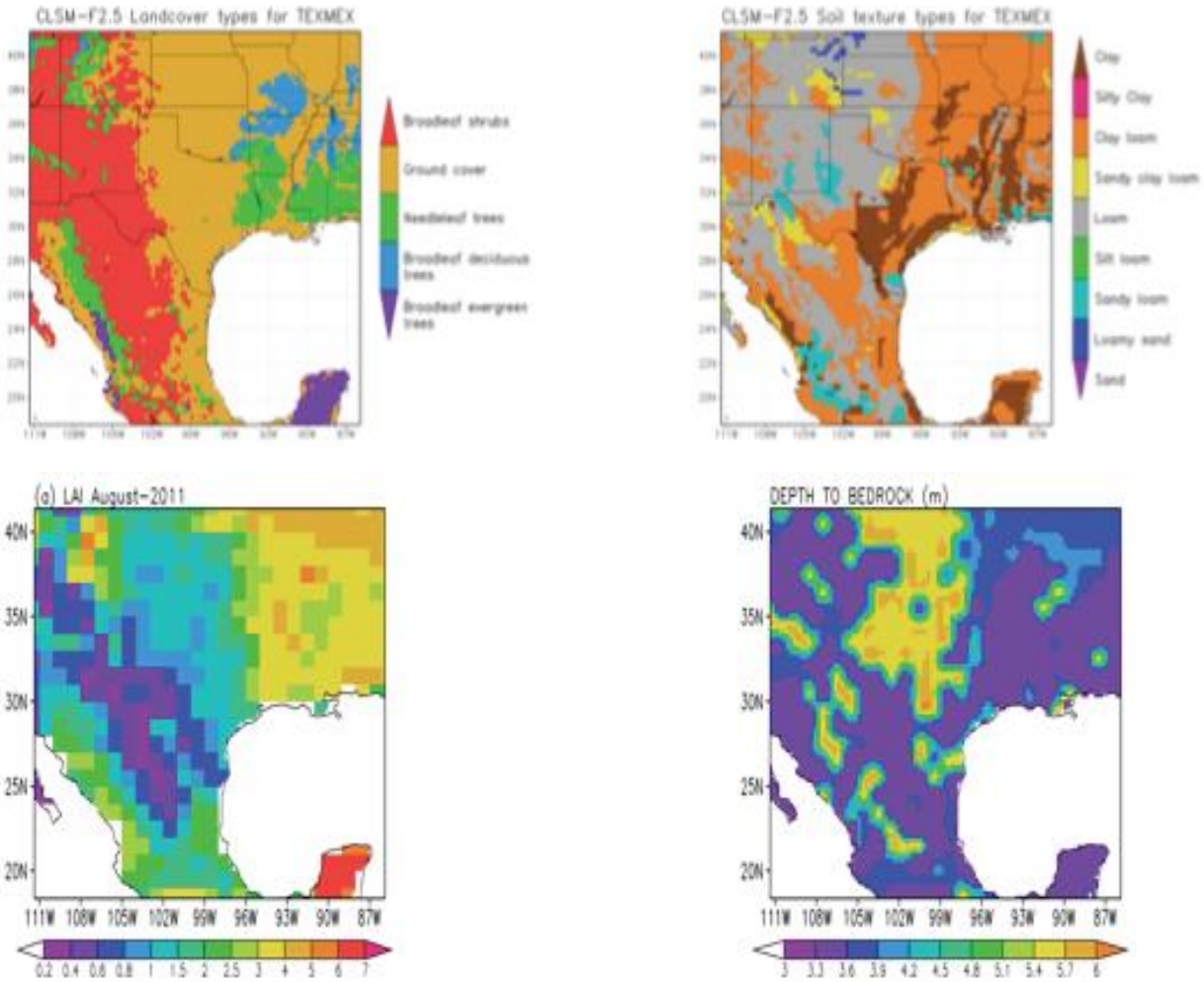

Figure 10. Same as Figure 9 but for TEXMEX domain and August instead of May LAI.

The LIS7/CLSM-f2.5 spinups were performed on a ¼ degree horizontal resolution grid and at 20-minute time steps using the procedure described above. The MERRA-Land meteorological forcing that was at a resolution of 1/2 degrees latitude × 2/3 degrees longitude and hourly was

bilinearly interpolated in space and time onto the ¼ degree x ¼ degree grid to perform the LIS7/CLSM-f2.5 spinups and open loop run.

2. Evaluations

In this section, we present our initial evaluation of the open loop runs over HOA. The objective of the initial evaluation was to confirm that the simulations were working correctly prior to initiating the data assimilation runs. The full results of our evaluation of the HOA and TEXMEX open loop runs are given in subsequent sections so that they can be directly compared with the data assimilation results.

For the HOA, the first step in our initial evaluation was to verify that the forcing data from MERRA-Land were properly read in and interpolated onto the ¼ degree grid. Figure 11 shows sample comparisons for precipitation, downward shortwave radiation, winds, and specific humidity. We also examined other forcing variables including longwave radiation and pressure, both as 2-d difference plots and time series plots. All these comparisons show only minor differences due to interpolation from the coarser MERRA-Land grid to the grid used in this project. Hence, we can conclude that the forcing processing for both the spinups and open loop runs worked properly.

The second step in our initial evaluation included a comparison of open loop outputs to the MERRA-Land outputs. Figure 12 shows sample outputs for evapotranspiration, surface runoff, subsurface runoff, and surface soil moisture. Similar to the input forcing outputs, these outputs suggest that there are only minor differences, due primarily to regridded forcing as well as parameters. A particular parameter difference that we investigated was the impact of the 2m increases in bedrock depth in our simulations relative to MERRA-Land. To assess the impact of this change, we calculated the error in the open loop Terrestrial Water Storage, which is the sum of groundwater, soil moisture and snow (if present), before and after lowering the bedrock depth. The error was calculated assuming GRACE TWS is truth. The results (not shown) indicated only small regions of significant change in error, hence we concluded that the benefits of the increase outweighed any costs.

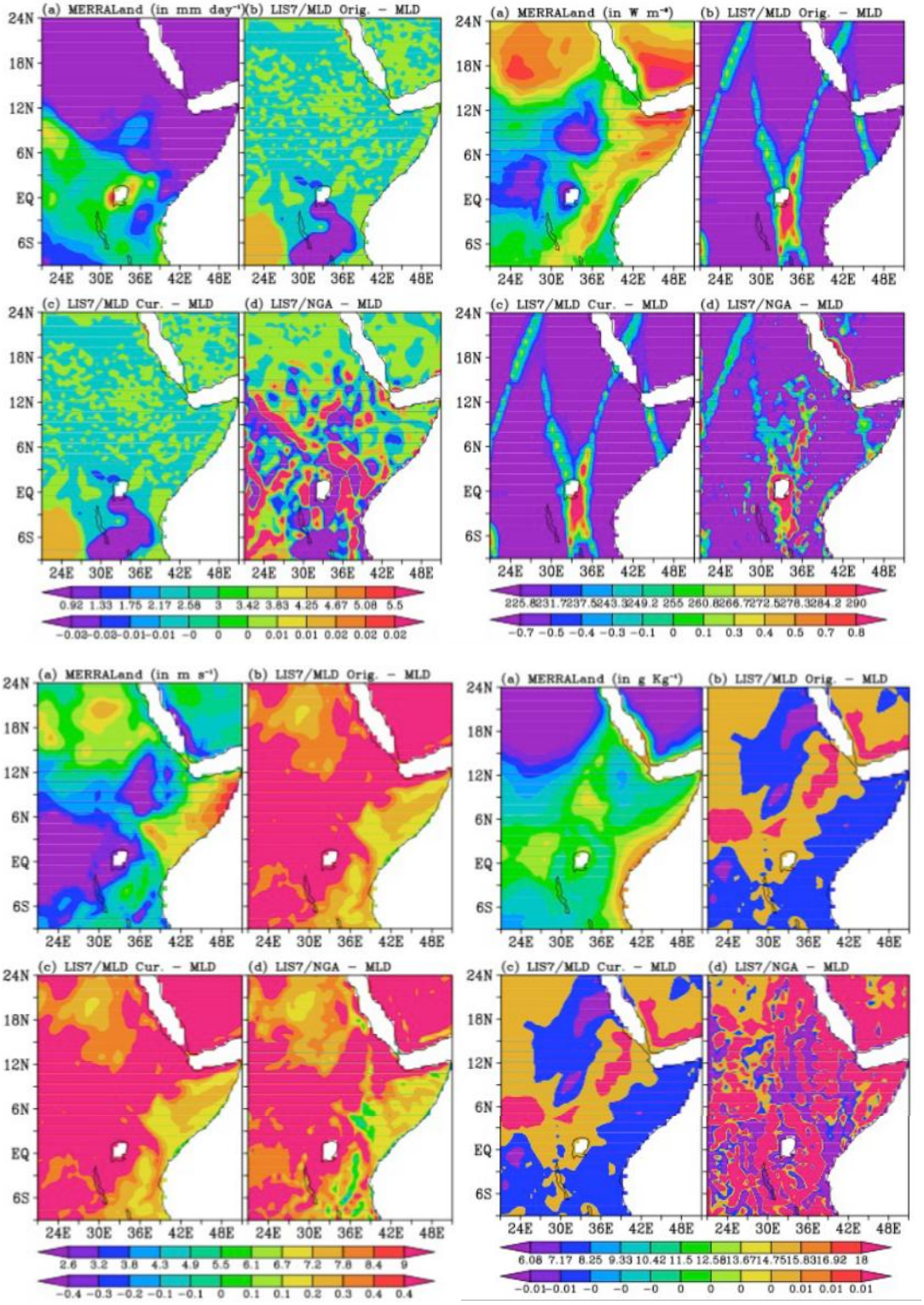

Figure 11. Comparison of forcings from MERRA-Land with interpolated forcings used in the open loop run for HOA. The forcings shown are (upper left) precipitation, (upper right) downward shortwave radiation, (lower left) wind speed, and (lower right) specific humidity.

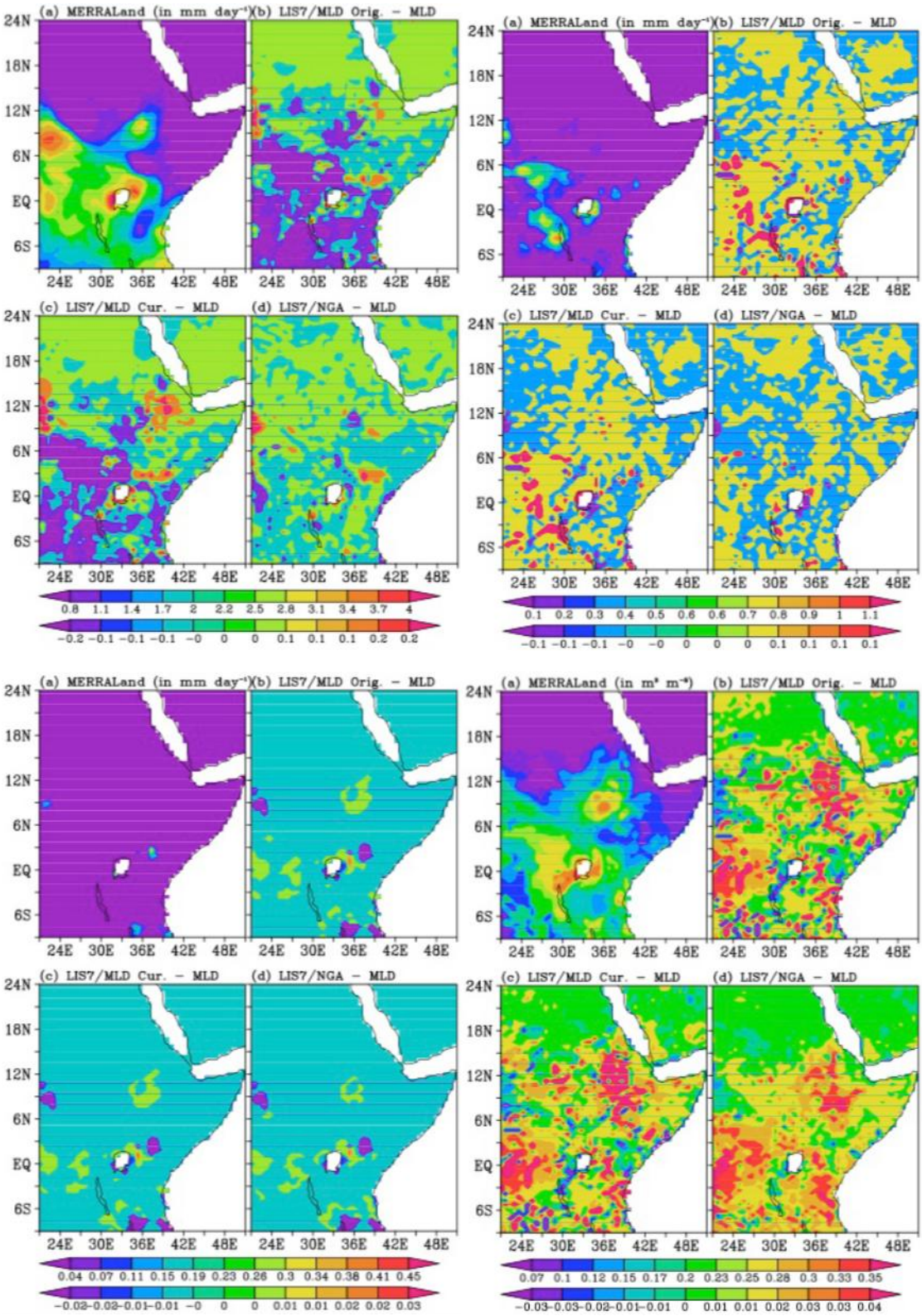

Figure 12. Comparison of MERRA-Land outputs and the equivalent outputs from our open loop run. The outputs shown are (upper left) evapotranspiration, (upper right) surface runoff, (lower left) subsurface runoff (baseflow), and (lower right) soil moisture.

C. Data Assimilation

1. AMSR-E Soil Moisture

Whereas in-situ measurements of soil moisture are very accurate at the local scale, achieving accurate regional soil moisture estimates derived solely from point measurements is difficult given the need for a dense gauge network and for the proper upkeep of these instruments, which can be costly. Microwave remote sensing is the only technology capable of providing timely direct measurements of regional soil moisture in areas that are lacking in-situ networks, such as the Horn of Africa region. Soil moisture remote sensing technology is well established has been successfully applied in many fashions to Earth Science applications (Schmugge, 1985; Jackson, *et al.*, 1982; Bolten *et al*., 2003) The basis for soil moisture retrieval from microwave measurements is made possible due to the large contrast between the dielectric constants of dry soil (~4) and water (~80). This contrast results in a broad range in the dielectric properties of soil-water mixtures (4 – 40), and is the primary influence on the natural microwave emission from the soil (Schmugge, 1985). Since the microwave emission from the soil surface is dependent upon the moisture content within the soil, when combined with physically-based models of the land surface via data assimilation, it is possible to derive accurate regional estimates of the soil column water content from microwave brightness temperature observed from satellite-based remote sensing instruments. In this project, we applied satellite-based estimates of soil moisture dynamics to improve the predictive capability of an optimized hydrologic model.

The soil moisture retrieval algorithm used in this study is the Land Parameter Retrieval Model (LPRM) - a radiative transfer-based approach to derive global land surface moisture and vegetation optical depth from satellite observations of microwave brightness temperature (Owe *et al.*, 2008; De Jeu and Owe, 2003; Meesters *et al*., 2005). Brightness temperature measured from space contains information on both the canopy and soil emissions and their respective physical temperatures. Polarization ratios, such as the Microwave Polarization Difference Index (MPDI), are frequently used to remove the temperature dependence, resulting in a parameter that is quantitatively and more highly related to the dielectric properties of the emitting surface(s). The MPDI is mainly a function of the overlying vegetation, and consequently a good indicator of the canopy density. However, at 6.9 GHz, the MPDI will not only contain information on the canopy, but will also contain significantly more information on the soil emission and consequently the soil dielectric properties. This approach is based, in part, on the theoretical relationship between the MPDI, vegetation optical depth, and the soil dielectric constant, and is described in Owe *et al*. (2001) and Meesters *et al*. (2005). The latter reference describes an analytical solution to this relationship, which improves the accuracy and overall efficiency of the retrieval algorithm, while also allowing one to modify model parameters such as surface albedo.

The LPRM retrieval methodology subsequently uses a nonlinear iterative optimization procedure in a forward modeling approach to partition the natural microwave emission from the Earth's

surface into its primary source components, *i.e.* the soil surface and the vegetation canopy. The model optimizes on the canopy optical depth and the soil dielectric constant. Once convergence between the calculated and observed brightness temperatures is achieved, the model uses a global data base of soil physical properties together with a soil dielectric mixing model (Wang and Schmugge, 1980) to solve for the surface soil moisture. No field observations of soil moisture, canopy biophysical properties, or other observations are used for calibration purposes, making the model largely physically-based and applicable at any microwave frequency suitable for soil moisture monitoring. Land surface temperature is also derived from high frequency satellite microwave measurements with a separate retrieval model. The application of the LPRM to AMSR-E observations is ideal for the TEXMEX and HOA regions because of the ability to apply both 6.9 GHz and 10.7 GHz, and its demonstrated sensitivity to soil moisture in the region (de Jeu *et al.*, 2008).

We applied near-daily surface soil moisture estimates derived from the satellite-based Advanced Microwave Scanning Radiometer (AMSR-E). The AMSR-E instrument on the NASA EOS Aqua satellite provides global passive microwave measurements of terrestrial, oceanic, and atmospheric variables for the investigation of global water and energy cycles (Njoku et al. 2003). The satellite follows a sun-synchronous orbit with equatorial crossing at approximately 1330 LST. The instrument measures brightness temperatures at six frequencies, 6.92, 10.65, 18.7, 23.8, 36.5, and 89.0 GHz, with vertical and horizontal polarizations at each frequency, for a total of twelve channels at an Earth incidence angle of 54.8°. With a fixed incidence angle of 54.8° and an altitude of 705 km, AMSR-E provides a conically scanning footprint pattern with a swath width of 1445 km. The mean footprint diameter ranges from 56 km at 6.92 GHz to 5 km at 89 GHz. The AMSR-E revisit coverage is obtained nearly every two days at the equator, independently for ascending and descending passes, and more frequently at higher latitudes. For the East Africa and Texas regions, the ascending and descending overpasses occur at approximately 130 and 1330 local time.

In the Catchment Land Surface Model (CLSM) [Koster et al., 2000], the vertical soil moisture profile is determined through deviations from the equilibrium soil moisture profile between the surface and the water table. Soil moisture in the 0–2 cm surface layer and in the 0–100 cm root zone layer is diagnosed from the modeled soil moisture states. The catchment LSM typically employs hydrologically defined catchments (or watersheds) as basic computational units. In this study, however, the catchment LSM is used on a regular latitude-longitude grid to facilitate the model intercomparison.

To integrate the AMSR-E observations with the NASA LIS CLSM, a data assimilation technique was used which applies auto-recursive analyses to optimally merge model estimates with state observations. The reduction in model uncertainty is achieved by taking advantage of model state temporal constancy restraints and model physical properties. Specifically, a 1-dimensional Ensemble Kalman filter (EnKF) was applied. The EnKF is a nonlinear extension of the standard

Kalman filter and has been successfully applied to land surface forecasting problems (Reichle et al., 2002). Within the filter, sequential ensembles of stochastically perturbed model trajectories are corrected towards an observation of model state when available. All the forcing and state perturbation parameters are given in Table 1. Our particular implementation of the EnKF integrates soil moisture observations from AMSR-E with the CLSM using a 1-dimensional EnKF at 20-minute model time-steps when AMSR-E observations are available. However, before the AMSRE soil moisture retrievals can be assimilated, the modeled and observed (AMSRE) data must be scaled to a common climatology to reduce potential biases and differences in dynamic range that commonly exist between modeled and observed surface soil moisture products. By removing time-invariant biases from the observation data, the two datasets can be optimally merged to allow more efficient assimilation (Reichle, et al., 2004). The removal of multiplicative and additive errors in this way also provides an objective basis for the comparison of soil moisture anomalies and a basis for properly validating the system.

Table 1. Parameters for perturbations to meteorological forcings and soil moisture prognostic model variables in the data assimilation integrations.

Variable	Perturbation Type	Standard Deviation	Cross Correlations with perturbations in Meteorological Forcings		
			Downward Shortwave	Downward Longwave	Precipitation
Downward Shortwave	Multiplicative	0.3 [-]	1.0	-0.5	-0.8
Downward Longwave	Additive	50 Wm^{-2}	-0.5	1.0	0.5
Precipitation	Multiplicative	0.5 [-]	-0.8	0.5	1.0
CLSM Soil moisture states					
			catdef	sfexc	
Catchment deficit (catdef)	Additive	0.05 mm	1.0	0.0	
Surface excess (sfexc)	Additive	0.02 mm	0.0	1.0	

The EnKF employed an ensemble size of 12, with perturbations applied to both the meteorological fields and model prognostic fields to simulate uncertainty in the soil moisture fields at ¼ degree grid resolution. The parameters used for these perturbations are listed in Table 1, which are based on earlier data assimilation studies (Kumar et al., 2009). As algorithms such as EnKF are designed to correct random, zero-mean errors and assume the use of unbiased observations relative to the model generated background, it is often a common practice to scale the observations prior to data assimilation to match the model's climatology (Reichle and Koster, 2004, Reichle et al., 2007, Kumar et al., 2009). Here we employed the Cumulative Distribution Function (CDF)-scaling approach of Reichle and Koster (2004), where the observations are rescaled to the model's climatology by matching the CDF of the observations to the CDF of the model soil moisture. The model CDF and observation CDF was computed using about 9 years of data separately for each grid point, from June 2002 to December 2011.

In this way, the AMSR-E retrievals are transformed such that their climatology is comparable to the climatology for top layer soil moisture estimates produced by the CLSM. The climatologically rescaled AMSRE data are then introduced as observations to the EnKF using sequential observations of AMSRE and climatological data. Each analysis was completed for the TEXMEX (111.25^{o}W-86.25^{o}W; 18.75^{o}N-41.25^{o}N) and Horn of Africa (HOA; 21.25^{o}E-51.25^{o}E; 11.25^{o}S-23.75^{o}N) regions.

2. GRACE Terrestrial Water Storage

The NASA/German Gravity Recovery and Climate Experiment (GRACE; Tapley et al., 2004) satellite mission measures month-to-month changes in Earth's gravity field, which can be used to infer changes in terrestrial water storage (TWS; the sum of groundwater, soil moisture, snow, ice, and surface waters). Challenges to using GRACE TWS data include their coarse spatial and temporal resolutions, their vertically integrated nature, and 2-5 month latency of the data products (Rodell et al., 2010). There is a trade-off between spatial resolution and accuracy, such that 150,000 km^2 is the approximate minimum area that can be resolved with a reasonable degree of confidence, although 1° x 1° resolution gridded TWS anomaly (deviation from the temporal mean) fields are distributed by NASA/JPL to facilitate delineation of a region of interest (Landerer and Swenson, 2012).

To address these challenges, Zaitchik et al. (2008) developed an Ensemble Kalman smoother (EnKS) data assimilation scheme to integrate GRACE and other data within the Catchment Land Surface Model (CLSM). The scheme merges basin-scale, monthly, and GRACE-derived TWS anomalies into CLSM using information on the uncertainty in both the observations and the model. It enables spatial and temporal downscaling by distributing the innovation (the difference between the observation and the model estimate of a state) among smaller spatial elements and time steps, and also acts to disaggregate the information vertically among water storage components. Results are fields of groundwater, soil moisture, and snow variations, which combine the veracity of GRACE with the fine spatial and temporal resolutions of the model.

Zaitchik et al. (2008) and Houborg et al. (2012) demonstrated that groundwater storage variability in several regions of the U.S. was more accurate in the GRACE assimilation than in the CLSM open loop results.

In an ensemble assimilation approach, conditional probability densities for predicted states are approximated by a finite number of model trajectories – the ensemble – with a covariance that reflects uncertainties in the model physics, parameters, and forcing data. Assimilation increments are calculated based on the relative uncertainty in the model and the observations, described by the (sample) error covariance matrices. The time-dependent Kalman gain matrix determines the relative weights of the model versus the observations during the update, and is defined on the basis of their respective covariance matrices. The error cross-covariance between the observed state and the model prediction is particularly important because it provides the basis for the distribution of information from the coarse scale observation to the finer scale model tiles. Since the cross-covariance matrix is diagnosed from the ensemble, the perturbations that are added to the forcings and state variables of each ensemble member must include realistic horizontal correlations. The ensemble update is computed separately for each GRACE observation. Prior to assimilation, the GRACE TWS anomalies are converted to absolute TWS values by adding the corresponding regional, time-mean water storage from the open loop portion of the CLSM simulation.

For the current project, the GRACE data assimilation approach developed by Zaitchik et al. (2008) was modified to enable assimilation of the 1° x 1° resolution gridded TWS anomaly fields directly, without first averaging them over large river basins. While each 1° pixel is not meaningful on its own (hence the basin averaging), there is useful spatial information in the GRACE fields at sub-basin scales. By carefully setting the observational error within the data assimilation scheme, we are able to preserve that spatial information while avoiding errors caused by overconfidence in the pixel scale GRACE data.

In the context of this project, the purpose of GRACE data assimilation is to improve the representation of soil moisture and groundwater in the model. These variables feed back to atmospheric processes, hence more accurate initialization of these fields in a coupled land-atmosphere forecast system should, all else being equal, increase forecast skill.

3. Evaluations

In this section, we evaluate the results from the Open Loop (OL), Soil Moisture Data Assimilation (DA-SM) and GRACE Terrestrial Water Storage Data Assimilation (DA-TWS) runs. Due to the lack of in situ data over HOA, the evaluation over that region focuses on remotely sensed evapotranspiration estimates, while over the TEXMEX domain we include both in situ and remotely sensed data in the evaluation. Note that these simulations do not represent forecasts; our evaluations of forecasted soil moisture come later.

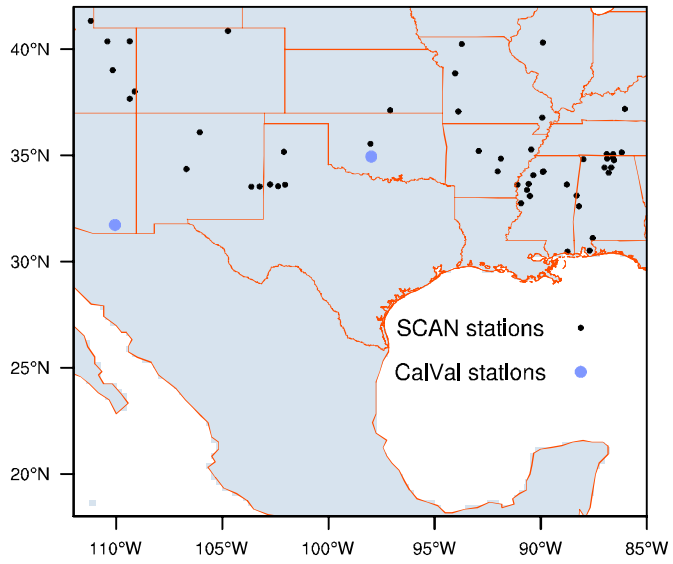

Figure 13. In situ soil moisture observations in the TEXMEX domain. The SCAN stations measure profiles while the ARS CalVal stations include only surface measurements in 2 experimental watersheds.

(a) TEXMEX

The soil moisture estimates from the simulations are compared against two reference datasets: (1) surface soil moisture measurements from four USDA Agricultural Research Service (ARS) experimental watersheds (Jackson et al. 2010) (two of which are in the modeled domain) and (2) soil profile measurements from the USDA Soil Climate Analysis Network (SCAN; Schaefer et al. 2007). The stations in the SCAN network provide hourly soil moisture measurements at the soil profile depths of 5, 10, 20, 50 and 100 cm, wherever possible. A number of extensive quality control procedures were applied to the raw data from the SCAN sites, the details of which are described in Liu et al (2011). We employ this quality-controlled dataset in our evaluations. Figure 13 shows the locations of the ARS and SCAN stations employed in the evaluations. These sites reflect the locations which passed the quality control of the in-situ data and where adequate soil moisture observations were assimilated.

Table 2 shows the comparison of the domain averaged anomaly correlation (R), anomaly root mean square error (RMSE) and unbiased RMSE metrics for the open loop and the DA integrations compared to the ARS and SCAN site data. The anomaly time series for each grid point is estimated by subtracting the monthly-mean climatology values from the daily average raw data, so that the anomalies represent the daily deviations from the mean seasonal cycle. (We thus do not measure the trivial skill associated with precipitation and evaporation seasonality.) The anomaly R and RMSE values are computed (separately at each grid point), as the correlation coefficient and RMSE between the daily anomalies from the assimilation estimates and the corresponding in-situ data, respectively. As the anomaly metrics are indifferent to any bias in the mean or amplitude of variations, the “unbiased” RMSE (ubRMSE), which is computed from the

time series after the removal of the long-term mean bias (Entekhabi et al. (2010), is also used as an evaluation metric. Due to the availability of SCAN and ARS datasets, the time period of Jan 2003 and December 2011 is used to compute these error metrics. In the evaluations, surface soil moisture is defined as the top 10cm of the soil column and the root zone is defined as the soil moisture content of the top 1m of the soil column (derived as a suitably weighted vertical average over the model and observation layers).

Table 2. Statistics of modeled soil moisture compared to in situ measurements at the SCAN and ARS sites. The model results shown include Open Loop (OL), Soil Moisture Data Assimilation (DA-SM) and GRACE Data Assimilation (DAGRACE).

Surface (SCAN)	OL	DA-SM	DA-TWS
Anomaly R	0.61 +/- 0.02	0.62 +/- 0.02	0.64 +/- 0.02
Anomaly RMSE	0.049 +/- 0.002	0.048 +/- 0.002	0.048 +/- 0.002
Unbiased RMSE	0.059 +/- 0.002	0.058 +/- 0.002	0.058 +/- 0.002

Root zone (SCAN)	OL	DA-SM	DA-TWS
Anomaly R	0.59 +/- 0.02	0.61 +/- 0.02	0.63 +/- 0.02
Anomaly RMSE	0.035 +/- 0.002	0.035 +/- 0.002	0.034 +/- 0.002
Unbiased RMSE	0.044 +/- 0.002	0.043 +/- 0.002	0.041 +/- 0.002

Surface (ARS)	OL	DA-SM	DA-TWS
Anomaly R	0.77 +/- 0.02	0.75 +/- 0.02	0.77 +/- 0.02
Anomaly RMSE	0.025 +/- 0.002	0.027 +/- 0.002	0.025 +/- 0.002
Unbiased RMSE	0.030 +/- 0.002	0.031 +/- 0.002	0.030 +/- 0.002

Table 2 indicates that both soil moisture and TWS assimilation helps in improving the soil moisture states. When compared to the SCAN measurements, the domain averaged open loop anomaly R is 0.61 and it provides a marginal improvement (not statistically significant) to 0.62 with soil moisture DA. The TWS assimilation shows a larger and statistically improvement in the surface soil moisture fields with the anomaly R of 0.64. In case of root zone soil moisture comparisons, the trends are similar, with soil moisture DA and TWS DA providing domain-averaged anomaly R values of 0.61 and 0.63, respectively compared to the open loop anomaly R value of 0.59. Similar trends of improvements are observed with the Anomaly RMSE and Unbiased RMSE metrics. In the comparisons to ARS data, the soil moisture DA shows a marginal degradation (in anomaly R) and TWS DA does not show any improvement. Note that only two watersheds from the ARS network are included in this evaluation, whereas the SCAN evaluation includes 55 stations.

The impact of data assimilation on the surface fluxes of latent and sensible heat are evaluated against four independent flux data products: (1) gridded FLUXNET data from the Max Plank Institute (MPI), which was created by synthesizing FLUXNET tower data with meteorological forcings and vegetation information from interpolated station and satellite data to produce a global, monthly, 0.5 degree resolution data product from 1982 to 2008 (Jung et al. 2009), (2) a global 1km ET estimate based on the MODIS satellite (Mu et al. 2011), (3) The Atmosphere-Land Exchange Inversion model (ALEXI) based flux products (Anderson et al. 2007), which are based on the thermal channel observations of the Geostationary Operational Environmental Satellites (GOES) and (4) a MODIS-based evapotranspiration product from the University of Washington (UW) (Tang et al. 2009).

Figure 14 shows the domain averaged difference maps of RMSE from the soil moisture and TWS DA integrations from the evaluations against the four reference datasets. The difference maps are computed by subtracting the RMSE of the DA integration from the RMSE of the open loop integration. If the difference is positive, then DA integration improves the open loop estimates and on the other hand, if the difference is negative, the DA integration degrades the open loop estimates.

Overall, degradations in the western part of the modeling domain are observed in the soil moisture DA comparisons. Most of the improvements from soil moisture DA are observed over the upper Mississippi basin. The changes in the ET fields due to TWS DA, on the other hand, is generally positive with improvements noted in Mexico and lower Mississippi basin. Figure 15 shows a similar comparison of the sensible heat fluxes from DA integrations compared against the FLUXNET and ALEXI datasets. Generally both DA integrations provide improvements in sensible heat fluxes, especially over the Mississippi basin areas.

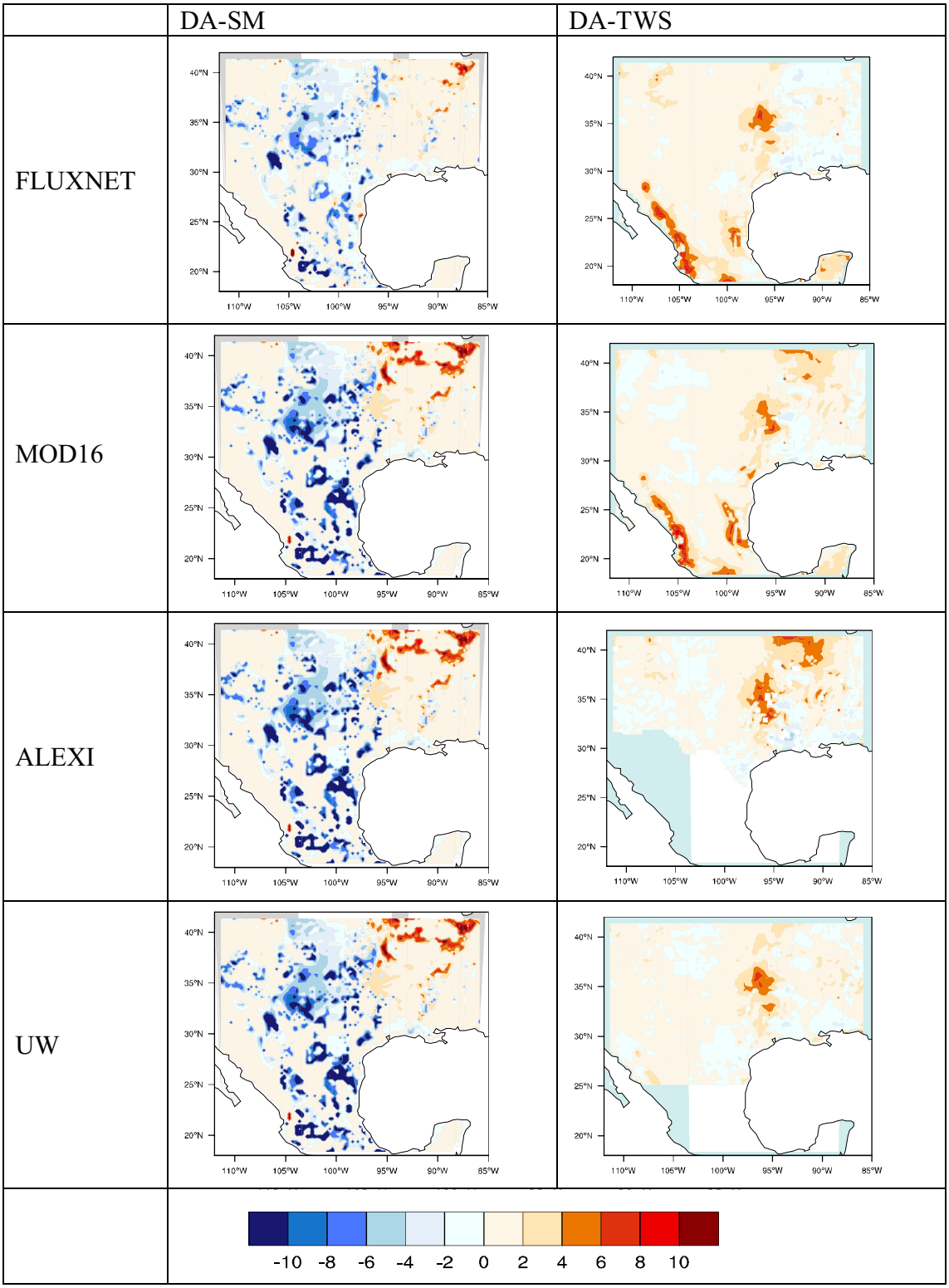

Figure 14: RMSE difference of latent heat flux estimates from soil moisture and TWS DA integrations compared against four reference datasets. The RMSE difference is computed as the RMSE of the open loop integration minus the RMSE of the DA integration. The blue (negative) colors indicate areas with degradation from DA and red (positive) colors indicate areas with improvements from DA.

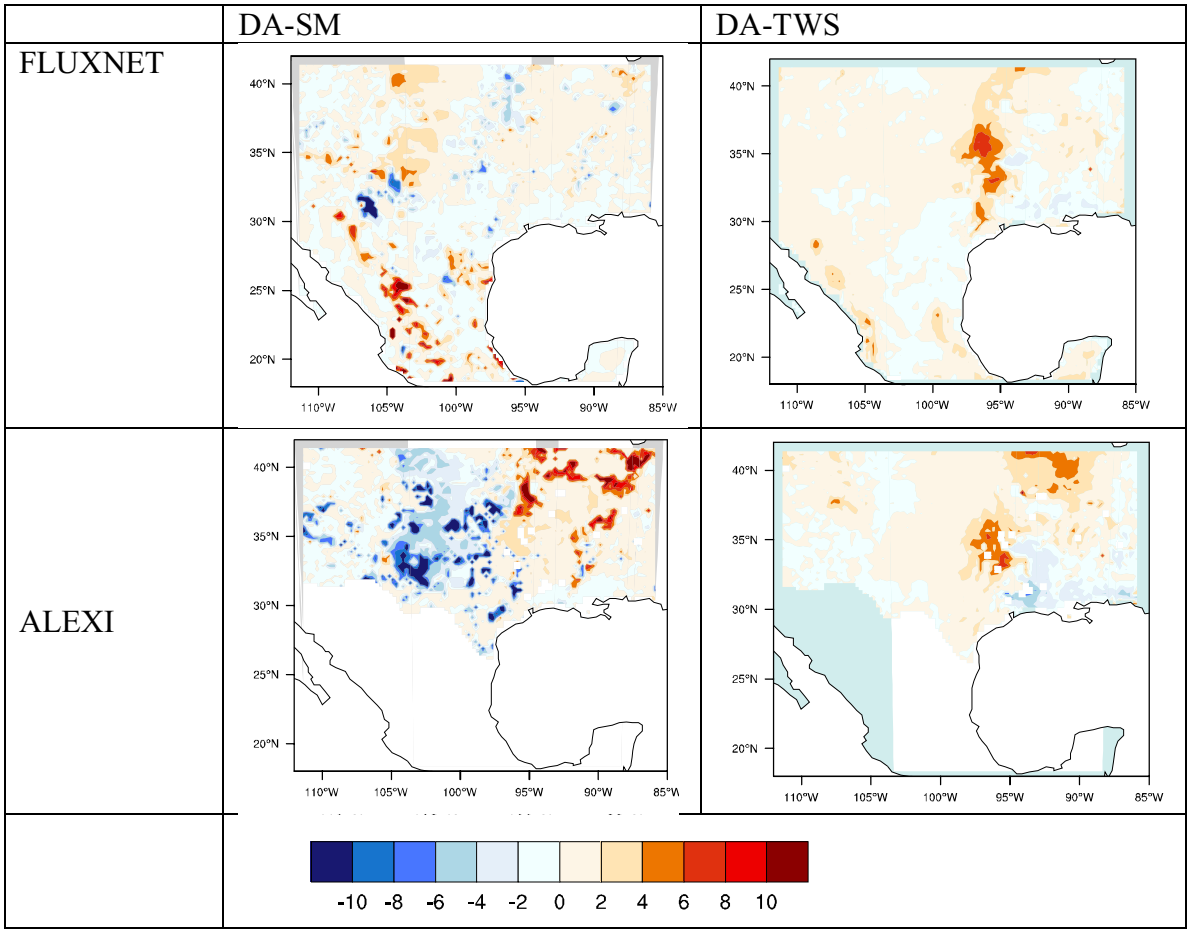

Figure 15: RMSE difference of sensible heat flux estimates from soil moisture and TWS DA integrations compared against four reference datasets. The RMSE difference is computed as the RMSE of the open loop integration minus the RMSE of the DA integration. The blue (negative) colors indicate areas with degradation from DA and red (positive) colors indicate areas with improvements from DA.

We conclude the evaluation of drought simulation in the TEXMEX region with a comparison against maps generated by the North American Drought Monitor (NADM). The plots on the left in Figure 16 show the percentiles of root zone soil moisture produced by the OL simulation during different months of 2011. (Percentiles are based on the monthly states produced over the full 31 years of simulation.) The plots on the right come directly from the published NADM. The color bar used for the OL percentiles was chosen to agree with the "drought severity classification" utilized by the drought monitor (http://droughtmonitor.unl.edu/classify.htm).

The salient result in the plot is the generally successful tracking of the NADM-defined drought, through its growth to its peak and decay, by the soil moisture percentiles produced with the LIS system. The agreement is indeed remarkable given that the NADM characterization of the drought is based on a number of indices (a subjective integration of precipitation, streamflow, reports from the field, etc.), whereas the OL root zone moisture percentiles shown in the figure represent a straightforward and fully objective calculation. The agreement gives us confidence that we capture the essential character of drought with our modeling system.

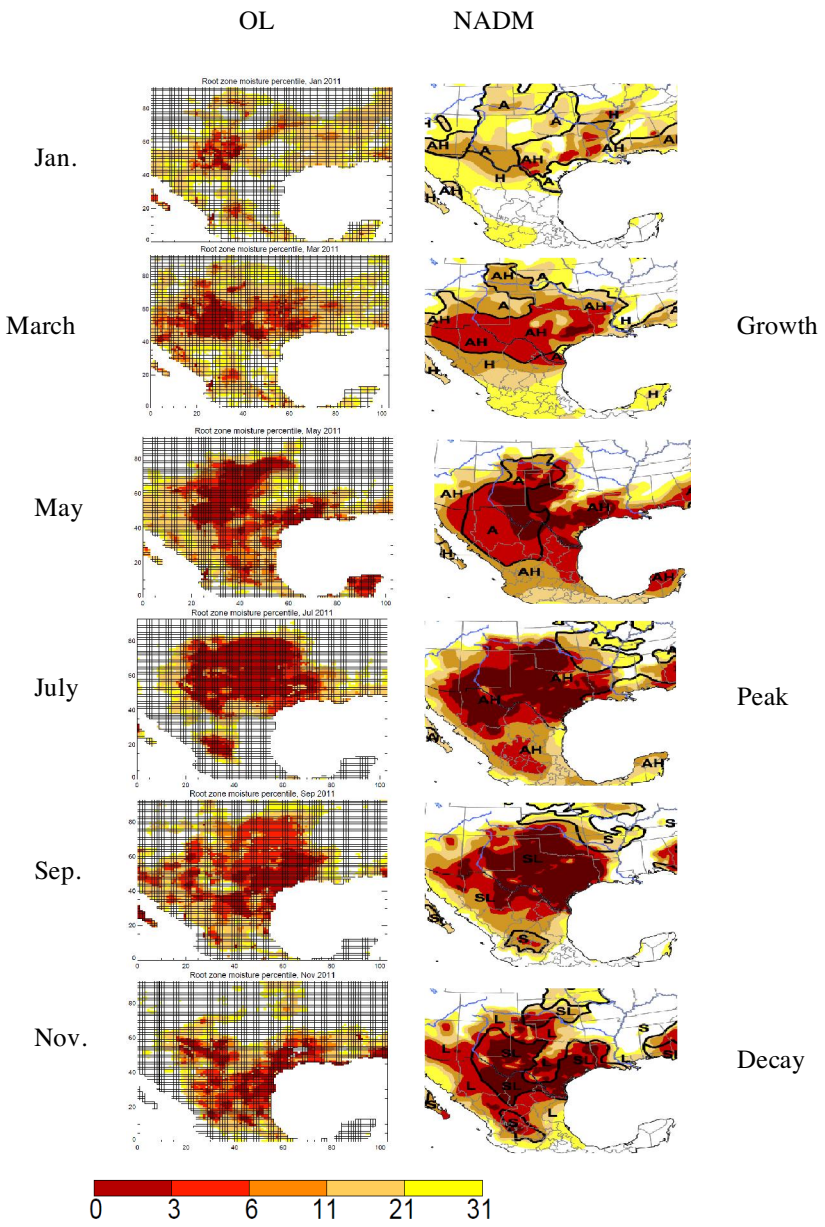

Figure 16. Percentiles of root zone soil moisture as produced by the OL simulation (right column) versus drought estimates published by the North American Drought Monitor (left column) for different phases of the 2012 TEXMEX drought.

The July 2011 root zone moisture percentiles produced in the OL simulations are compared to those produced in the DA-TWS simulation in Figure 17. While some small differences are seen, particularly in the neighborhood of Mississippi, the assimilation of GRACE TWS data has generally a small impact on estimated drought.

July 2011 soil moisture percentile, OL simulation

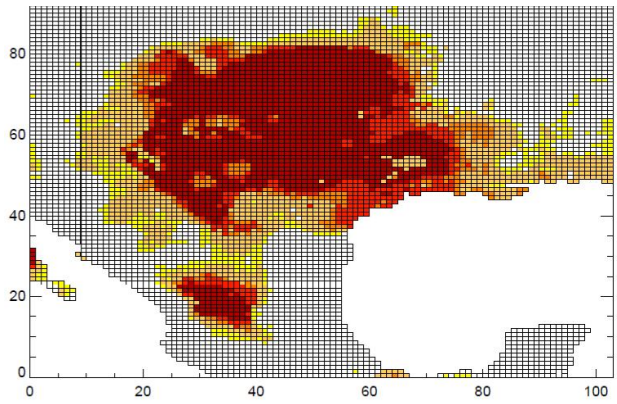

July 2011 soil moisture percentile, DA-TWS simulation

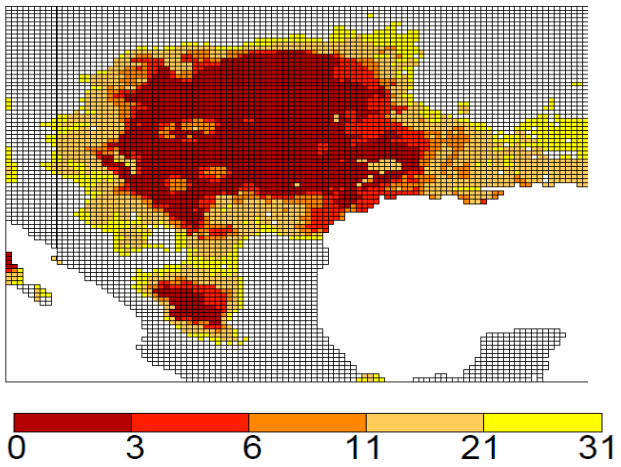

Figure 17: Impact of data assimilation (in particular, the assimilation of TWS estimates from GRACE) on the computed estimate of root zone moisture percentiles for July 2011.

(b) HOA

Due to the lack of adequate ancillary measurements over HOA, the evaluations are limited to comparisons against FLUXNET, MOD16, NDVI, and FEWSNET-based datasets .

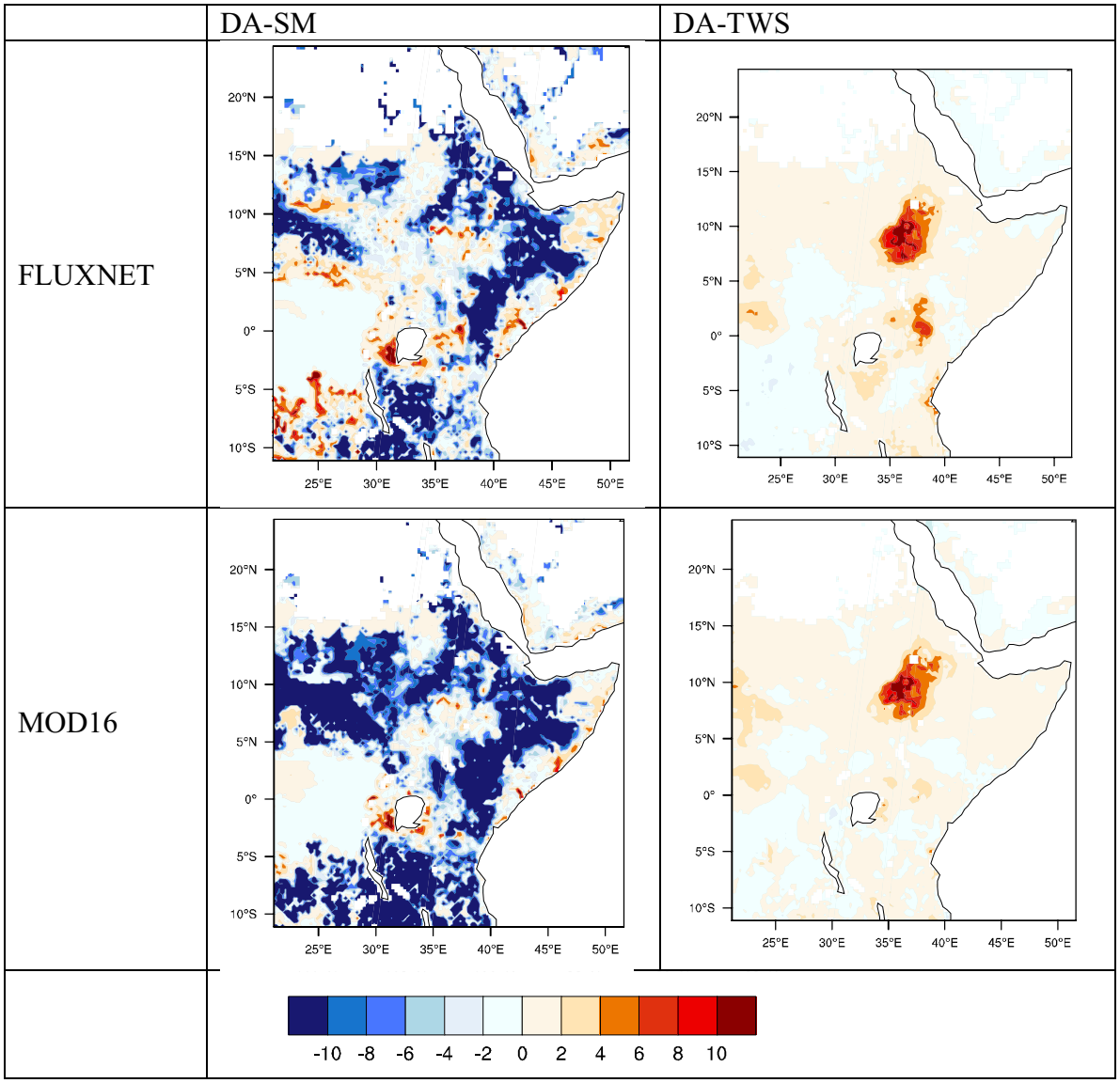

Figure 18: RMSE difference of latent heat flux estimates from soil moisture and TWS DA integrations compared against two reference datasets. The RMSE difference is computed as the RMSE of the open loop integration minus the RMSE of the DA integration. The blue (negative) colors indicate areas with degradation from DA and red (positive) colors indicate areas with improvements from DA.

Similar to the results shown over the TEXMEX domain, the evaluation of the ET fields given in Figure 18 indicates degradations from soil moisture DA over several parts of the domain, with a few areas of improvement such as the Horn, areas near Uganda and Tanzania. The TWS improvements are mostly over the wetland region in Sudan known as the Sudd.

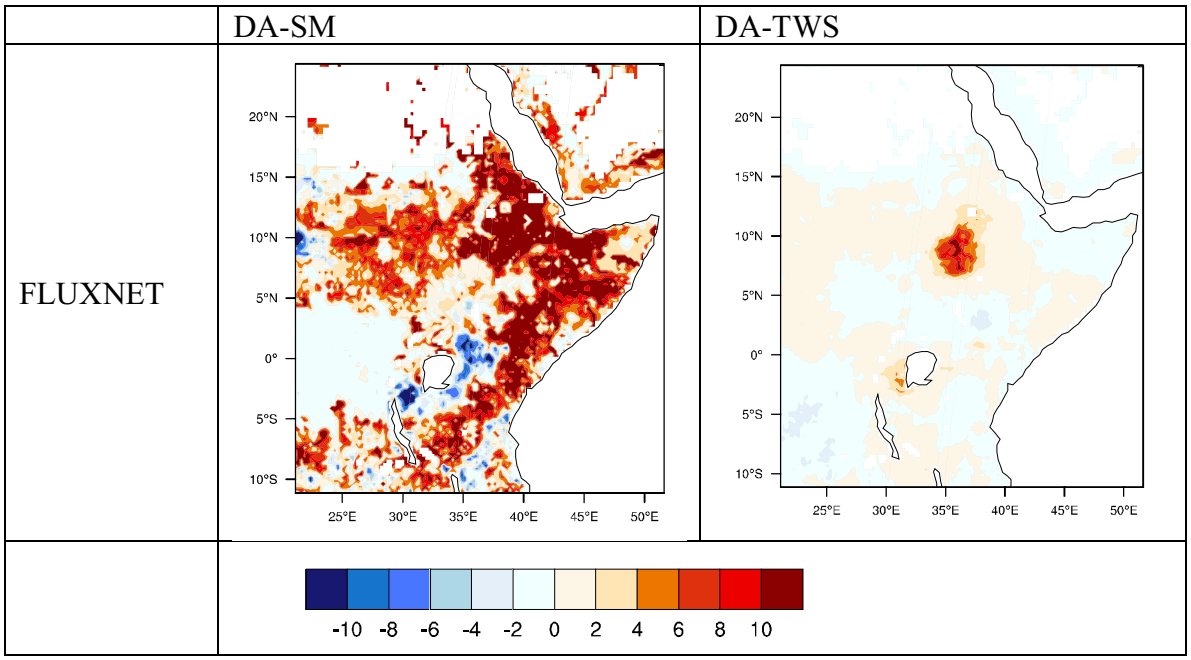

Figure 19: RMSE difference of sensible heat flux estimates from soil moisture and TWS DA integrations compared against FLUXNET data. The RMSE difference is computed as the RMSE of the open loop integration minus the RMSE of the DA integration. The blue (negative) colors indicate areas with degradation from DA and red (positive) colors indicate areas with improvements from DA.

The evaluation of the sensible heat fluxes from DA integrations against the FLUXNET data is shown in Figure 19. In most parts of the domain, soil moisture DA provides improvements in the sensible heat flux fields with the TWS DA again providing improvements over the Sudd.

Note that the reference ET datasets themselves have associated uncertainties, and our independent analysis (not shown) of the products showed that MOD16 systematically underestimates fluxes and likely has higher uncertainties associated with it. The FLUXNET product, on the other hand is developed from sparse tower network data.

In analogy to Figures 16 and 17 for the TEXMEX region, the root zone soil moisture percentiles for the HOA region are presented in Figure 20. The first column shows the percentiles for April, the peak of the HOA drought. Africa does not have a useful equivalent of the NADM, so to evaluate these patterns, we turn to an NDVI map for May (second column of Figure 20). A negative NDVI anomaly is indicative of reduced vegetation coverage and/or lushness, which in turn serves as a useful indicator of low soil moisture in the weeks leading up to the measurement. The large negative anomaly inside the blue circle generally agrees with the low soil moisture percentiles produced there by both the OL and DA-TWS simulations in April. Note that simulated soil moisture percentiles are especially affected by GRACE data assimilation in the area highlighted by the green circle.

The third column of Figure 20 shows the simulated percentiles of root zone moisture in the HOA region for the April-June period, the peak of the growing season in Somalia. Results are in fact shown only in a subset of the region, that area for which we have data on crop water requirement satisfaction index (WRSI) from the Famine Early Warning Systems Network (FEWS-NET) (fourth column). The crop WRSI represents the amount of soil water available during the growing season of the major crop—in this case maize—where deficits represented by an index value less than 50 represent crop failure. The model simulations accurately capture the failure of crops in the area enclosed by the magenta circle. The simulations show dryness toward the west where crops were successful; perhaps this is because agriculture toward the west (unlike in Somalia) is dominated by production in other seasons.

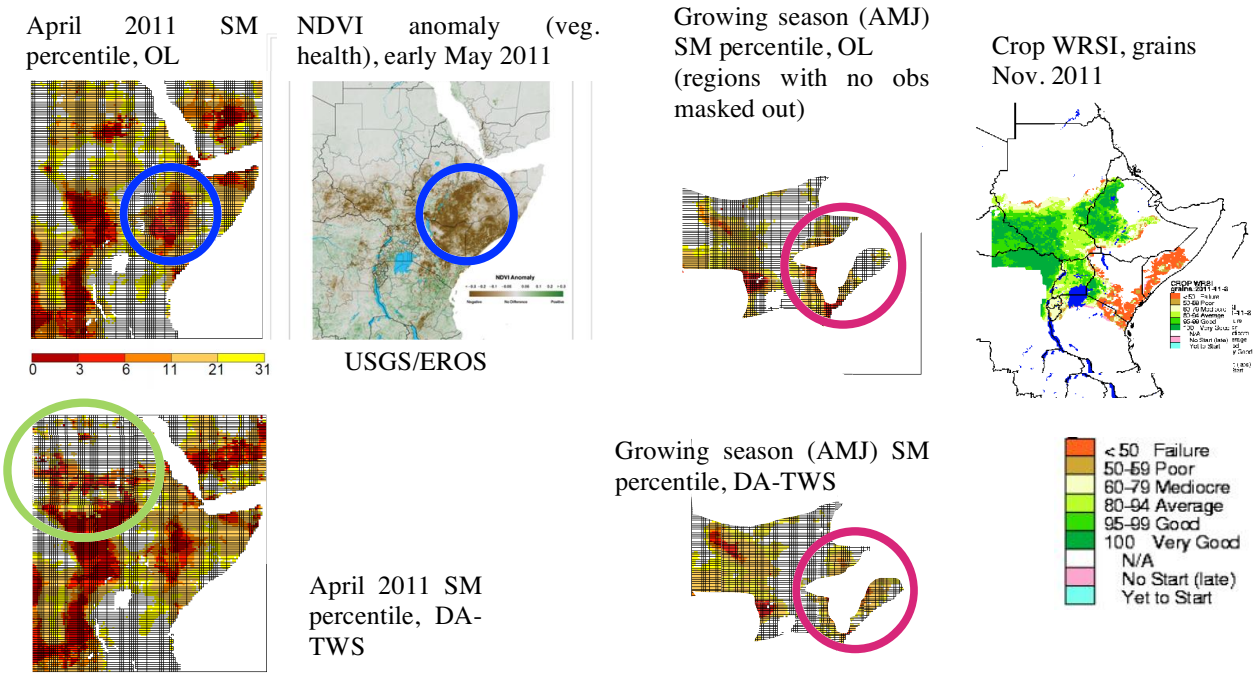

Figure 20: First column: root zone soil moisture percentiles for April as produced in the OL simulation (top) and the DA-TWS simulation (bottom). Second column: NDVI anomaly for the first part of May. Third column: root zone soil moisture percentiles for the April-June period as produced in the OL simulation (top) and the DA-TWS simulation (bottom). Fourth column: end-of-year estimates of crop failure in the HOA region, as estimated by the FEWS-NET WRSI model. For ease of comparison, masks are applied in the third column to mimic the regions of data availability shown in the fourth column. The circled areas are discussed in the text.

D. GEOS-5 Forecast Experiments

1. Experiment Setup

The HOA and TEXMEX regions exhibited severe drought conditions in the year 2011. The following three sets of LIS7 experiments were performed to examine the drought prediction skill obtained by utilizing different land surface initial conditions with GEOS5 forecasts: (i) LIS7 forecasts initialized with the open loop runs described in Section II.B. (OL), (ii) LIS7 forecasts initialized after performing soil moisture data assimilation from Advanced Microwave Scanning Radiometer-Earth (AMSR-E: Owe et al. 2008) Observing System's/Land Parameter Retrieval Model (LPRM) from 2002-2011 (DA-SM, described above) and (iii) LIS7 forecasts initialized with after performing terrestrial water storage data assimilation based on the Gravity Recovery And Climate Experiment (GRACE: Houborg et al. 2012) from 2003-2011 (DA-TWS, described above).

Based on our assessment of GEOS-5 prediction skill, we determined that one- to three-month forecasts would be the limit at which we would expect reliable drought forecasts. Therefore, one- to three- month forecasts were performed in all the experiments to target each month in the year 2011 up to 3 months. For example, to have January 2011 as the 3rd -month target-forecast, the experiments were performed by initializing LIS7 at the beginning of November 2010. Figure 19 illustrates the overview of the forecasted months during 2010 and 2011 in each experiment.

(a) Meteorological forcing data

The meteorological forcing data in conducting LIS7/CLSM-f2.5 retrospective forecasts up to 9-lead months were extracted from GEOS5 forecasts. The meteorological data used to force the land component of GEOS5 (CLSM) during the production of forecasts were archived at 1.25^{o}longitude x 1^{o} latitude resolution and at half hour frequency (Table 3). The total precipitation-forcing fields from the GEOS5 forecasts were found to be different (mostly higher) from the MERRA-Land precipitation for all the seasons. To correct this bias, new precipitation forcing is estimated by CDF matching (Reichle and Koster, 2004) wherein the precipitation climatology of each ensemble member of GEOS5 forecasts is rescaled to match the climatology of MERRA-Land precipitation.

(b) LIS7 experiments

The meteorological forcing from GEOS-5 that was at a resolution of 1.25^{o}×1^{o} and 30-min frequency is bilinearly interpolated in space and time to 0.25^{o} and 15-min, respectively, to perform the LIS7/CLSM-f2.5 experiments. The LIS7/CLSM-f2.5 experiments (OL, DA-SM, and DA-TWS) differ from each other only in their initial conditions. The initial conditions for the 'OL' forecasts were extracted from the LIS7/CLSM-f2.5 experiment OL run covering 1981 to 2011. As previously described, the initial conditions for the OL run were produced with a 62-year spin-up of the LIS7/CLSM-f2.5 system. The initial conditions for the DA-SM and DA-TWS

forecasts were obtained from experiments that were performed by assimilating AMSR-E/LPRM soil-moisture and GRACE TWS in OL runs, respectively.

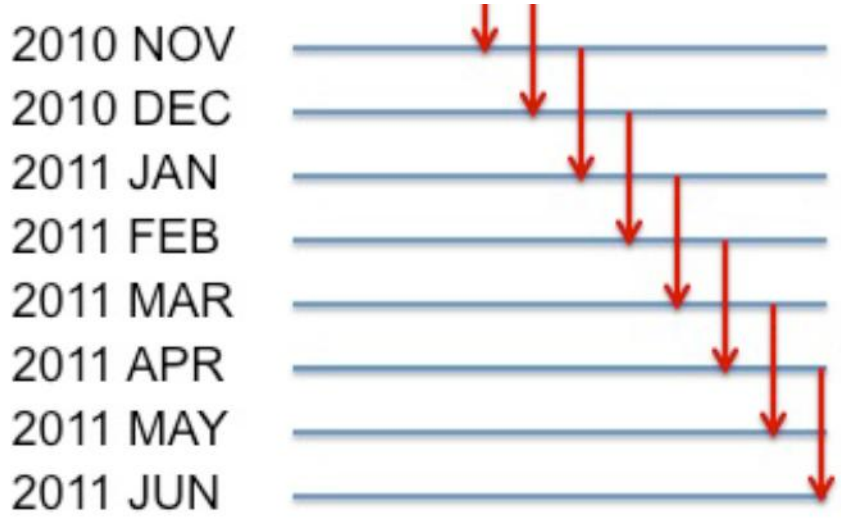

Figure 21. The red solid arrows show the 3-month forecasts by initializing at the month indicated at the beginning of the arrow. Various initialized months and forecast lengths are so chosen to target-forecast each month in the year 2011 up to 3 months.

Note that the catchment parameters used in the LIS7/CLSM-f2.5 experiments (OL, DA-SM and DA-TWS) differ from those used in the GEOS5/CLSM forecasts. The following differences are found between the LIS7/CLSM and GEOS5/CLSM forecasts:

(1) The horizontal spatial resolution of the domain for LIS7/CLSM-f2.5 is 0.25^{o}, whereas the GEOS5/ CLSM-f2.5 simulations were performed at $1.25^{o} \times 1^{o}$ horizontal spatial resolution.
(2) The time step used in the LIS7/CLSM-f2.5 simulations is 15 minutes, whereas a 30-minute time step was used in the GEOS5/ CLSM-f2.5 simulations.
(3) The turbulence scheme used in LIS7 is the Louis scheme (Louis 1979), whereas GEOS5 used the Helfand scheme (Helfand and Labraga 1988; Helfand et al. 1999).
(4) CLSM-f2.5 simulations were performed on tile space in GEOS5 and on grid space in LIS7.
(5) The bedrock depths are deeper by 2m in the LIS7/CLSM-f.2 experiments. Some catchment parameters (e.g., total water holding capacity) are altered by this change.

Table 3. The meteorological forcing data from GEOS5 used in LIS7 simulations.

GEOS5 forcing data
1. Near Surface Air Temperature (K) 2. Near Surface Specific Humidity (Kg Kg^{-1}) 3. Incident Shortwave Radiation (W m^{-2}) 4. Incident Longwave Radiation (W m^{-2}) 5. Eastward Wind (m s^{-1}) 6. Northward Wind (m s^{-1}) 7. Surface Pressure (Pa) 8. Rainfall Rate (Kg m^{-2} s^{-1}) 9. Snowfall Rate (Kg m^{-2} s^{-1}) 10. Convective Rainfall Rate (Kg m^{-2} s^{-1}) 11. Height of Forcing Variables (m) 12. Photosynthetically Active Direct Radiation (W m^{-2}) 13. Photosynthetically Active Diffuse Radiation (W m^{-2}) 14. Net Shortwave Radiation at the Surface (W m^{-2})

2. Evaluations

(a) Soil Moisture

Spatial maps of the LIS7/CLSM root zone soil moisture forecasts in the HOA region for the peak of the drought period are presented in Figure 20 (first three columns, each column representing a different forecast start date). The percentiles shown can be compared to those from the OL simulation (fourth column) and to the aforementioned NDVI data (fifth column). The forecast system does predict dry conditions for April in many parts of the HOA region, even when initialized at the beginning of February. Only the forecast initialized at the beginning of April, however, captures reasonably well the precise locations of many of the anomalies seen in the OL simulation and in the NDVI data.

While an improvement in forecast skill with a reduction in lead-time is not a surprise, it is also worth emphasizing here the nature of an ensemble forecast. The forecast results in Figure 21 represent an average over seven separate soil moisture forecasts (based on an ensemble of seven meteorological forecasts from GEOS5), each reflecting a possible trajectory of soil moisture evolution over the HOA region. Nature, in contrast, provides only one trajectory. Shown in Figure 21 are seven soil moisture forecasts for April, each one initialized at the beginning of March. The two forecast maps with the overlain blue circles indicate the key point – for the March 1 initialization, some of the ensemble members capture the dryness seen in the observations, whereas others do not. Taking the ensemble mean "washes out" the extreme signals produced by some ensemble members. While this is an unavoidable facet of ensemble

forecasting, because we have no way of knowing a priori which ensemble member will be the most accurate, the existence of the desired signal amongst the ensemble should be kept in mind. (Note: in all of the plots featuring ensemble averages, the percentiles are defined based on a ranking of the ensemble mean forecasts; thus, dry extremes can show up for the ensemble mean even given the averaging process.)

Figure 22 provides a summary of the results. The ensemble mean forecast of April root zone moisture was averaged over the area enclosed by the red square, and the resulting large-scale forecasts (in terms of percentiles for the ensemble averages) are shown for different start dates and different lead times in the final three columns (red lines). Shown for comparison are the corresponding OL simulation results (black lines); while these cannot be interpreted as "truth", because they are products of the same model, they are nevertheless presumably close enough to the truth to be useful. Of particular interest are the results in the bottom row, which corroborate some of the findings already discussed – the model is able to predict drier conditions for April in the indicated region even as early as February. The model also predicts well the wet conditions seen in mid-2010 (top row).

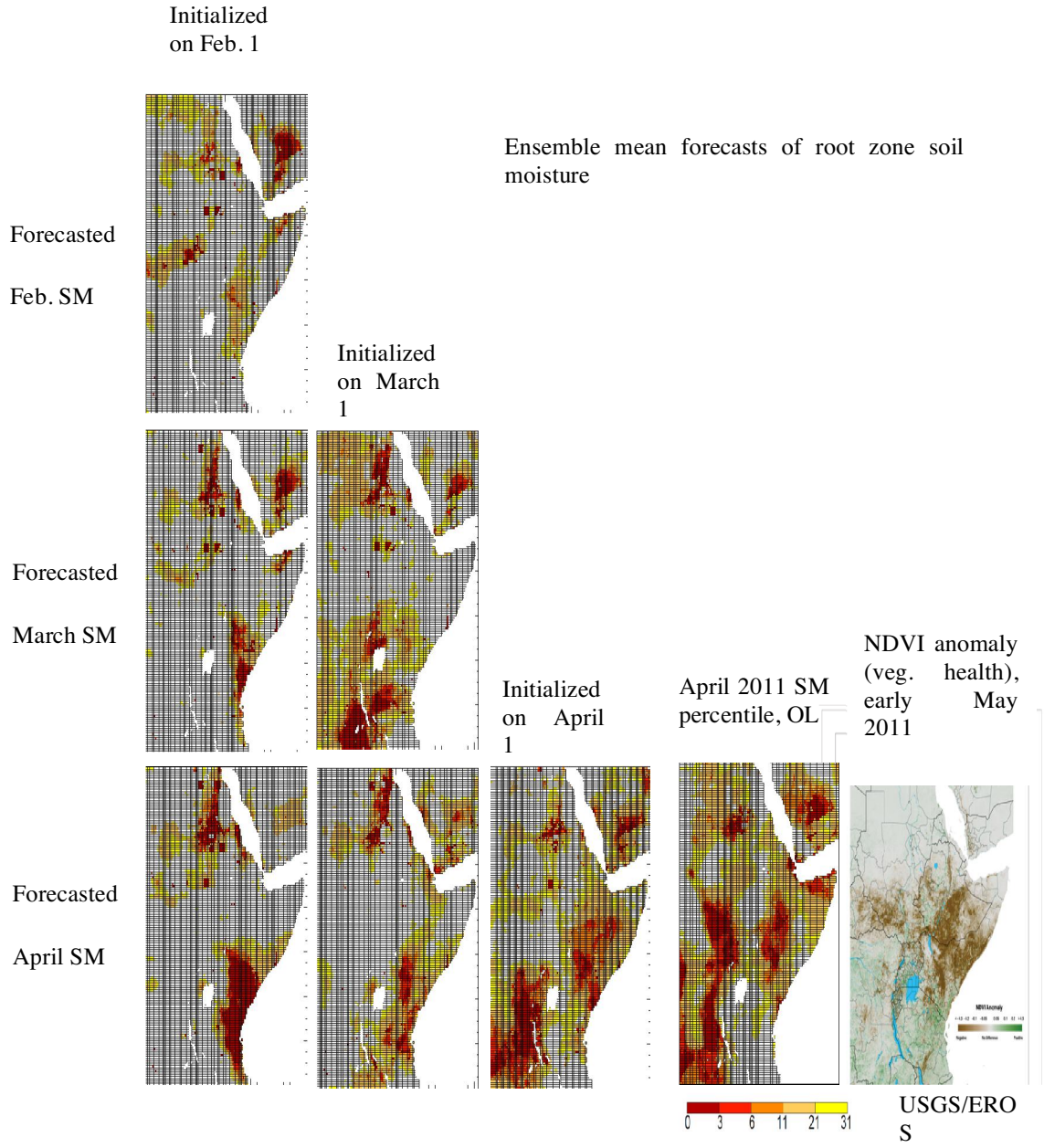

Figure 22: Columns 1-3: Root zone soil moisture forecasts for different forecast initialization dates, expressed as percentiles. The April forecasts (lowest panel in each of these columns) can be compared to the OL simulation results (Column 4) and the NDVI data (Column 5).

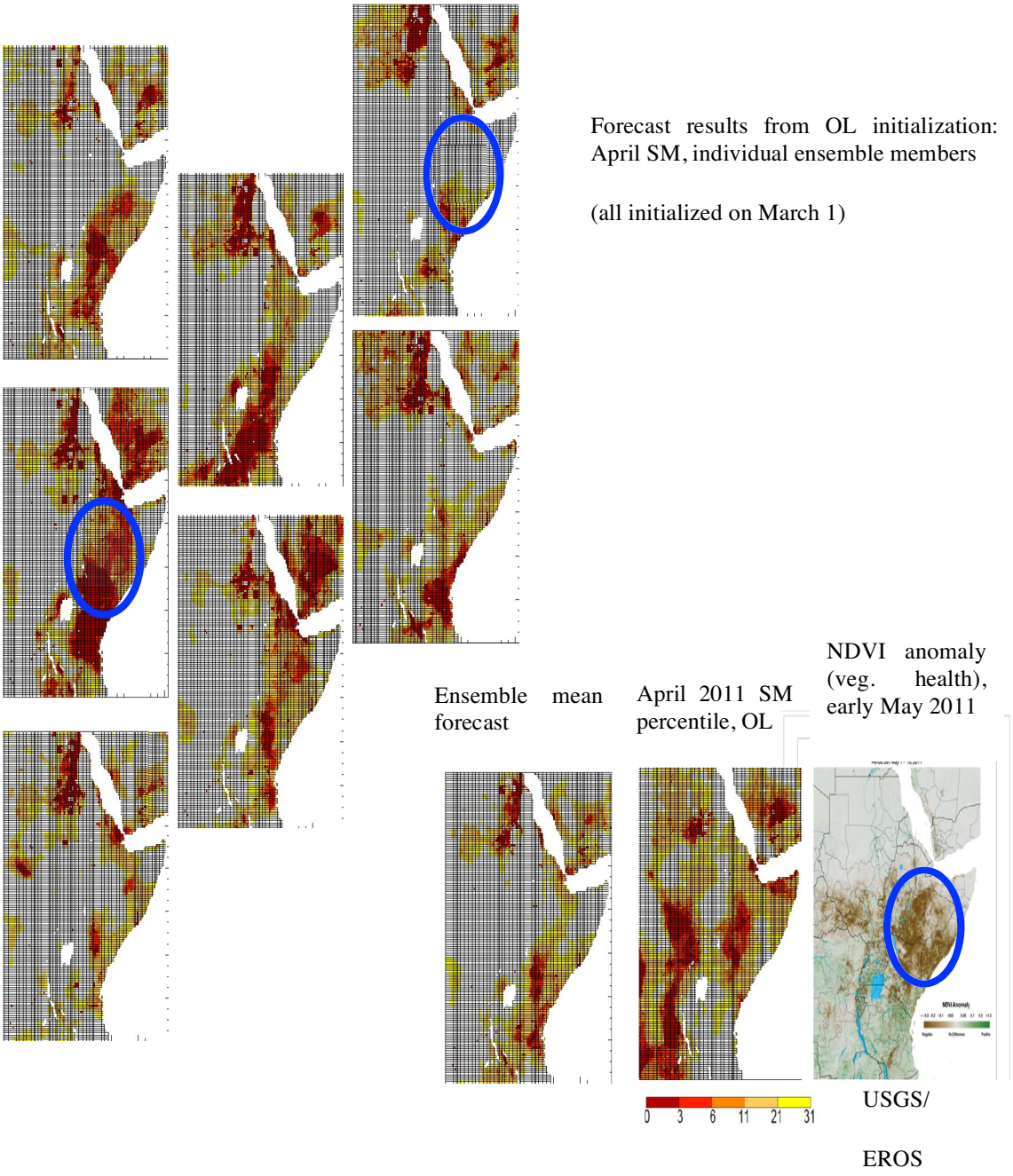

Figure 23: Root zone soil moisture forecasts for April (expressed as percentiles) as produced by the seven different forecast ensemble members, each initialized on March 1. The three panels in the lower right show, respectively, the ensemble mean forecast for April, the April percentiles produced in the OL simulation, and the observed NDVI anomaly for early May.

NDVI anomaly (veg. health), early May 2011

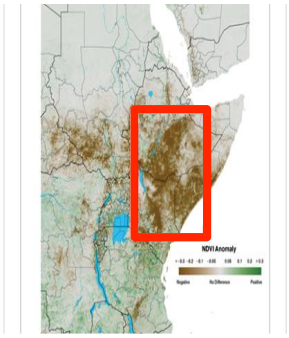

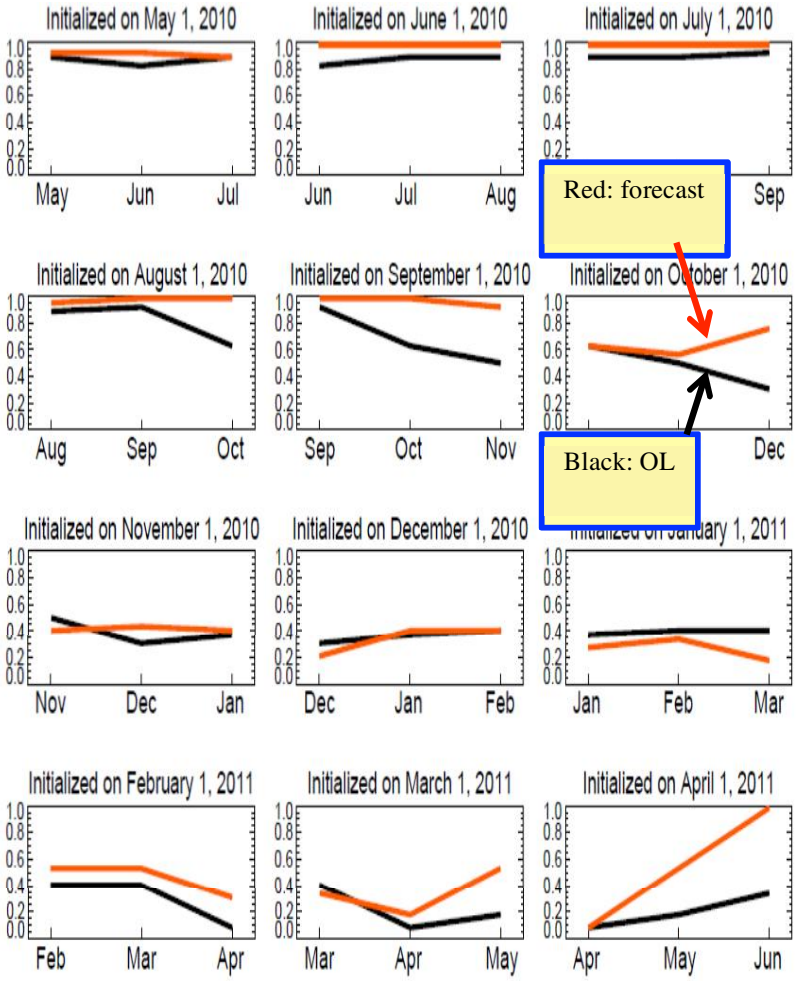

Figure 24: Forecasted root zone soil moisture percentiles for the indicated region (bounded by the red square) for different start dates (different panels) and lead times (x-axis within each panel). The forecasts are shown as red lines; an estimate of the true percentiles, as derived from the OL simulation, are shown in black lines.

(b) Human Migration

Simulated soil moisture at 0.25°×0.25° can be analyzed alongside estimates of human migration. The human migration dataset was derived by our project partners at CRREL based on the Population Movement Trends (PMT) portal (UNHCR, 2013) and provides drought-induced population movement datasets reported by the source district of the displacement, at monthly intervals from January 2008 to September 2012. The resolution and location of gridded GEOS-5 forecast products required a method of assigning grid cells to the geographic units of interest in a given statistical analysis. In the case of the PMT datasets, these units of interest are Somali

administrative units at the district level. Because the spatial resolutions of the model grid cells are similar to those of Somali administrative districts, grid cells were assigned to a specific district when at least half of the area of the grid cell fell within that district's boundary. Subsequently, the seven districts that were not large enough to intersect more than half of any one grid cell were manually assigned one or more grid cells that best represented the spatial extent of the district. Here we divide the IDP (internally displaced persons) count by the local population density and thus work with normalized migration (human displacement) data.

A caveat is necessary here. We do not claim to provide a predictive equation for human migration based on our simulations – the available data for migration (4 years) are simply too limited for adequate statistical analysis. The correlations shown below should be considered as qualitative rather than quantitative, and they are not necessarily indicative of a causal relationship. That said, the correlations do suggest that a predictive equation may exist and could be established, given the collection of more data.

We computed correlations, for three different averaging periods (1 months, 2 months, and 3 months), between normalized migration and four quantities:

1) The root zone soil moisture during the month prior to the averaging period, as determined from the open loop simulation (i.e., using the prior month's moisture as the predictor of migration).

2) Same as (1), but as determined from the simulation using GRACE data assimilation.

3) The root zone soil moisture for the averaging period produced during the open loop simulation (i.e., using a "best possible" estimate of moisture as the predictor, in the absence of assimilation.)

4) Same as (3), but as produced in the simulation using GRACE data assimilation.

In all cases, a mean seasonal cycle is subtracted from the soil moisture and migration data prior to the correlation calculations. This seasonal cycle is necessarily very crude, given the 4-yr period examined. Note that correlations with the 3rd and 4th quantities above are presented for reference only; these soil moisture quantities, which rely on known precipitation and/or GRACE measurements during the forecast period, are not true forecasts.

Figure 25 shows the results. Negative correlations (blue colors) indicate a migration of people away from an area during times of lower-than-average soil moisture (i.e., drought-induced migration). Several features of Figure 25 stand out: (i) the blue colors generally dominate the yellow colors, suggesting a general correlation in the expected direction; (ii) The correlations are nevertheless generally small, though some larger values appear in certain areas; (iii) The correlations do not improve on average when the "correct" precipitation is applied (3rd and 4th columns), though they do improve significantly in some locations; (iv) Correlations are smallest for the 1-month averaging period; and (v) In general, the correlations are not generally stronger

when GRACE data are used rather than the open loop data. Again, all of these features are suggestive rather than conclusive; a proper statistical analysis would require substantially more data.

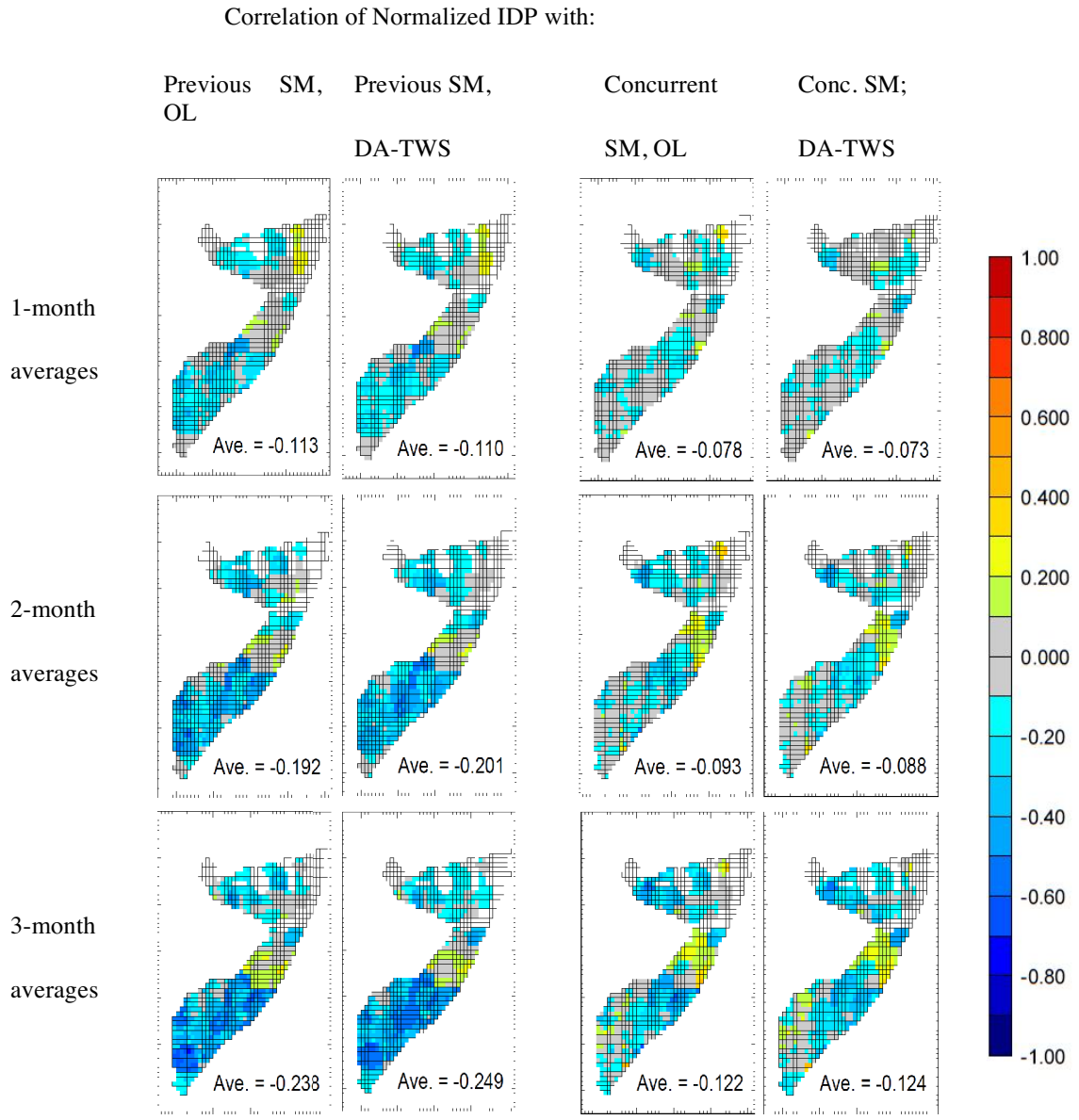

Figure 25. First column: correlation between a soil moisture predictor (the soil moisture in the month prior to the averaging period, from the OL simulation) and the normalized human displacement during the averaging period. Negative correlations are consistent with the idea that drought induces migration. Second column: Same, but for the soil moisture predictor taken from the DA-TWS simulation. Third column: same, but for the soil moisture predictor set to the soil moisture produced by the OL simulation during the averaging period (i.e., not representing a forecast). Fourth column: same, but for the soil moisture predictor set to the soil moisture produced by the DA-TWS simulation during the averaging period (again, not a forecast).

E. Summary

This work set out to answer the question: "Can existing, linked infrastructures be used to predict the onset of drought months in advance?" Based on our work, the answer to this question is "yes" with the qualifiers that skill depends on both lead-time and location, and especially with the associated teleconnections (e.g., ENSO, Indian Ocean Dipole) active in a given region/season.

As part of this work, we successfully developed a prototype drought early warning system based on existing/mature NASA Earth science components including the Goddard Earth Observing System Data Assimilation System Version 5 (GEOS-5) forecasting model, the Land Information System (LIS) land data assimilation software framework, the Catchment Land Surface Model (CLSM), remotely sensed terrestrial water storage from the Gravity Recovery and Climate Experiment (GRACE) and remotely sensed soil moisture products from the Aqua/Advanced Microwave Scanning Radiometer – EOS (AMSR-E). We focused on a single drought year—2011—during which major agricultural droughts occurred with devastating impacts in the Texas-Mexico region of North America and the Horn of Africa.

Our results demonstrate that GEOS-5 precipitation forecasts show skill globally at 1-month lead, and can show up to 3 months skill regionally in the TEXMEX and HOA areas. Our results also demonstrate that the CLSM soil moisture percentiles are a good indicator of drought, as compared to the North American Drought Monitor for TEXMEX and a combination of FEWS-NET data and MODIS NDVI anomalies over HOA.

The data assimilation experiments produced mixed results. Neither soil moisture nor evaporation was significantly improved after assimilating AMSR-E soil moisture products. Hence, soil moisture assimilation was not found to significantly impact the ability of CLSM to monitor drought, as expressed via soil moisture percentiles. In contrast, the GRACE terrestrial water storage (TWS) assimilation was found to significantly improve soil moisture and evapotranspiration, as well as drought monitoring via soil moisture percentiles.

We carried out 1-3 month lead time forecast experiments using archived and properly rescaled GEOS-5 forecasts as input to LIS/CLSM with the three uncoupled simulations (OL, DA-SM, and DA-TWS) as initial conditions. Based on these forecast experiments, we find that the differences between the OL, DA-SM and DA-TWS initial conditions are not significant, but that the expected skill in GEOS-5 forecasts from 1-3 months is present in the soil moisture percentiles used to indicate drought. In the case of the HOA drought, the failure of the long rains in April appears in the February 1, March 1 and April 1 initialized forecasts, suggesting that for this case, drought forecasting would have provided some advance warning about the drought conditions observed in 2011.

F. Recommendations

Drought forecasting skill is unique to each model, region and season, and requires an understanding of the teleconnections that lead to predictable patterns of temperature and precipitation over a given area. This study was focused on developing a prototype drought forecasting system based on existing NASA science. While the initial results are promising, the system was evaluated for a single set of droughts observed in 2011 over two regions: the Texas-Mexico drought over North America and the Horn of Africa drought. *Hence, our first recommendation is to carry out a comprehensive analysis of droughts observed over the entire period of record for GEOS-5 forecasts.*

A key finding of this work is that the ability of GEOS-5 to capture the Indian Ocean Dipole can lead to 1-3 month predictions of drought in the Horn of Africa. As noted in the discussion on GEOS-5, these teleconnections can lead to skill in both the long rains and short rains, with GEOS-5 suggesting a higher probability of predicting anomalies in the short rains. *Another recommendation would be to continue to analyze the GEOS-5 forecasts in HOA stratifying by anomalies in long and short rains to better quantify the skill for these key seasonal cycles of rainfall and crop production for the HOA region.*

Finally, the hypothesis that the GRACE Terrestrial Water Storage data assimilation and the Aqua/AMSR-E soil moisture data assimilation would improve drought prediction by providing better initial conditions was not supported by our results. We did show that GRACE TWS assimilation improves soil moisture and potentially drought monitoring. However, a single year of analysis is inadequate to fully demonstrate whether this information provides a benefit or not. Newer sensors such as the ESA Soil Moisture/Ocean Salinity (SMOS) and the upcoming NASA Soil Moisture Active/Passive (SMAP) mission to be launched in Fall 2014 should provide deeper soil moisture information that should be valuable. *Therefore, a final recommendation is to continue to include GRACE TWS and SMOS/SMAP soil moisture products in a routine activity building on this prototype to further quantify the benefits for drought assessment and prediction.*

III. REFERENCES

Behera, S. K., J.-J. Luo, S. Masson, P. Delecluse, S. Gualdi, A. Navarra, and T. Yagamata, 2005: Paramount impact of the Indian Ocean dipole on the East African short rains: A CGCM study. J. Climate, 18, 4514–4530, doi:10.1175/JCLI3541.1.

Bolten, J., Lakshmi, V., Njoku, E., (2003) "Soil moisture retrieval using the passive/active L and S- band radar/radiometer." IEEE Transactions on Geoscience and Remote Sensing, vol. 41, pp. 2792-2801.

Cosgrove, B. A., et al. (2003), Land surface model spin-up behavior in the North American Land Data Assimilation System (NLDAS), J. Geophys. Res., 108, 8845, doi:10.1029/2002JD003316, D22.

De Jeu, R.A.M. and M. Owe, (2003) "Further validation of a new methodology for surface moisture and vegetation optical depth", *Int. J. Remote Sens.*, **24**:4559-4578, doi: 10.1080/0143116031000095934.

De Jeu, R.A.M, WW Wagner, TRH Holmes, AJ Dolman, NC van de Giesen, and J Friesen. (2008) Global Soil Moisture Patterns Observed by Space Borne Microwave Radiometers and Scatterometers, *Surveys in Geophysics*, doi 10.1007/s10712-008-9044-0.

Ducharne, A., R.D. Koster, M.J. Suarez, M. Stieglitz, and P. Kumar, 2000: A catchment-based approach to modeling land surface processes in a GCM, Part 2, Parameter estimation and model demonstration, J. Geophys. Res., 105, 24823-24838, doi: 10.1029/2000JD900328

Griffies, S.M. and Coauthors, 2005: Formulation of an ocean model for global climate simulations. Ocean Science,45-79.

Harrison, K. W., S. V.Kumar, C. D. Peters-Lidard, and J. A.Santanello, 2012: Quantifying the change in soil moisture modeling uncertainty from remote sensing observations using Bayesian inference techniques, Water Resour. Res., 48, W11514, doi:10.1029/2012WR012337.

Helfand, H. M., and J. C. Labraga, 1988: Design of a nonsingular level 2.5 second-order closure model for the prediction of atmospheric turbulence. *J. Atmos. Sci*, **45,** 113–132, doi: http://dx.doi.org/10.1175/1520-0469(1988)045<0113:DOANLS>2.0.CO;2

Helfand, H. M., A. Molod, and M. G. Bosilovich, 1999: Implications of a moist turbulence parameterization for the numerical prediction of the structure and properties of the atmospheric boundary layer. Preprints, *13th Conf. on Numerical Weather Prediction,* Denver, CO, Amer. Meteor. Soc., 54–59.

Houborg, R., M. Rodell, B. Li, R. Reichle, and B. Zaitchik, 2012: Drought indicators based on model assimilated GRACE terrestrial water storage observations, Wat. Resour. Res, 48, W07525, doi:10.1029/2011WR011291.

Jackson, T.J., T.J. Schmugge, and J.R. Wang, (1982). "Passive microwave sensing of soil moisture under vegetation canopies". *Water Resources. Res.,* **18(4)**:1137-1142.

Koster, R. and M. Suarez, 1996: Energy and Water Balance Calculations in the Mosaic LSM, NASA Technical Report Series on Global Modeling and Data Assimilation 104606, Vol. 9.

Koster, R.D., M.J. Suárez, A. Ducharne, M. Stieglitz, and P. Kumar, 2000: A catchment-based approach to modeling land surface processes in a GCM, Part 1, Model Structure. J. Geophys. Res., 105, 24809-24822, doi: 10.1029/2000JD900327.

Kumar, S. V., C. D. Peters-Lidard, Y. Tian, P. R. Houser, J. Geiger, S. Olden, L. Lighty, J. L. Eastman, B. Doty, P. Dirmeyer, J. Adams, K. Mitchell, E. F. Wood and J. Sheffield, 2006. Land Information System - An Interoperable Framework for High Resolution Land Surface Modeling. Environmental Modelling & Software, 21, 1402-1415, doi: 10.1016/j.envsoft.2005.07.004.

Kumar, S. V., Peters-Lidard, C. D., Santanello, J., Harrison, K., Liu, Y., and Shaw, M., 2012b: Land surface Verification Toolkit (LVT) – a generalized framework for land surface model evaluation, Geosci. Model Dev. Discuss., 5, 229-276, doi:10.5194/gmdd-5-229-2012.

Kumar, S., C.D. Peters-Lidard, J.L. Eastman, and W.-K. Tao, 2008: An Integrated High Resolution Hydrometeorological Modeling Testbed using LIS and WRF, Environmental Modelling & Software, 23(2), 169-181, DOI:10.1016/j.envsoft.2007.05.012.

Kumar, Sujay V., Rolf H. Reichle, Randal D. Koster, Wade T. Crow, Christa D. Peters-Lidard, 2009: Role of subsurface physics in the assimilation of surface soil moisture observations, J. Hydrometeor., 10: 1534-1547 doi:10.1175_2009JHM1134.1.

Kumar, S. V., R. H. Reichle, K. W. Harrison, C. D. Peters-Lidard, S. Yatheendradas, and J. A. Santanello, 2012a: A comparison of methods for a priori bias correction in soil moisture data assimilation, Water Resour. Res., 48, W03515, doi:10.1029/2010WR010261.

Kumar, Sujay V., Rolf H. Reichle, Christa D. Peters-Lidard, Randal D. Koster, Xiwu Zhan, Wade T. Crow, John B. Eylander, and Paul R. Houser, 2008. A Land Surface Data Assimilation Framework using the Land Information System: Description and Applications, Adv. Water Resour., 31(11), 1419-1432, doi:10.1016/j.advwatres.2008.01.013.

Landerer F.W. and S. C. Swenson, 2012: Accuracy of scaled GRACE terrestrial water storage estimates. Water Resources Research, Vol 48, W04531, 11 PP, doi:10.1029/2011WR011453.

Liu, Yuqiong, Christa D. Peters-Lidard, Sujay Kumar, James L. Foster, Michael Shaw, Yudong Tian, Gregory M. Fall, 2013: Assimilating satellite-based snow depth and snow cover products for improving snow predictions in Alaska, Advances in Water Resources, 54, 208-227, doi: 10.1016/j.advwatres.2013.02.005.

Louis, J-F.: 1979, A Parametric Model of Vertical Eddy Fluxes in the Atmosphere,Boundary-Layer Meteorol. 17, 187–202, doi: 10.1007/BF00117978.

Meesters, A.G.C.A., R.A.M. de Jeu, and M. Owe, 2005: "Analytical derivation of the vegetation optical depth from the microwave polarization difference index", *IEEE Trans. Geoscience and Remote Sensing,* **2(2)**:121-123.

Njoku, E.G., T.L. Jackson, V. Lakshmi, T.Chan, and S.V. Nghiem, 2003: Soil moisture retrieval from AMSR-E, IEEE Transactions on Geoscience and Remote Sensing, 41 (2): 215-229.

Owe, M., R.A.M. de Jeu, and J. Walker, 2001: "A methodology for surface soil moisture and vegetation optical depth retrieval using the microwave polarization difference index", *IEEE Trans. Geosci. and Remote Sensing,* **39**:1643-1694

Owe, M., R.A.M. de Jeu, and T.R. H. Holmes, 2008: Multi-sensor historical climatology of satellite-derived global land surface moisture, J. Geophys. Res. 13, F01002, doi:1029/2007JF000769.

Peters-Lidard, C.D., P. R. Houser, Y. Tian, S.V. Kumar, J. Geiger, S. Olden, L. Lighty, B. Doty, P. Dirmeyer, J. Adams, K. Mitchell, E. F. Wood, and J. Sheffield (2007), "High performance Earth system modeling with NASA/GSFC's Land Information System, Innovations in Systems and Software Engineering, 3(3), pp 157-165.

Peters-Lidard, C. D., Kumar, S. V., Mocko, D. M. and Tian, Y., (2011) Estimating evapotranspiration with land data assimilation systems. Hydrological Processes, 25: 3979–3992. doi: 10.1002/hyp.8387.

Reichle, R.H. and R.D. Koster, 2004: Bias reduction in short records of satellite soil moisture, Geophys. Res. Lett., 31, L19501, doi10.1029 /2004GL020938.

Reichle, R.H., D.B. McLaughlin, and D. Entekhabi, 2002: Hydrologic data assimilation with the Ensemble Kalman Filter. *Mon. Wea. Rev.*, vol. 130, pp. 103-114, doi: http://dx.doi.org/10.1175/1520-0493(2002)130<0103:HDAWTE>2.0.CO;2.

Reichle, R.H., S.V. Kumar, S.P.P. Mahanama, R.D. Koster and Q. Liu, 2010: Assimilation of satellite-derived skin temperature observations into land surface models, J. Hydrometeor., 11,1103-1122,doi:10.1175/2010JHM1262.1.

Reichle, R. H., R. D. Koster, G. J. M. De Lannoy, B. A. Forman, Q. Liu, S. P. P. Mahanama, and A. Toure, 2011a: Assessment and enhancement of MERRA land surface hydrology estimates, *Journal of Climate*, 24, 6322-6338, doi:10.1175/JCLI-D-10-05033.1.

Reichle, R. H., 2012: The MERRA-Land Data Product. GMAO Office Note No. 3 (Version 1.2), 38 pp, available at http://gmao.gsfc.nasa.gov/pubs/office_notes.

Reichle, R. H. and Coauthors, 2011b: GMAO Research Highlights: The MERRA-Land data product, available at http://gmao.gsfc.nasa.gov/research/landsurface/highlights/GMAO_2011Highlights_Reichle_et_al_MERRA-Land.pdf

Rienecker, M.M., and Coauthors, 2008: The GEOS-5 Data Assimilation System - Documentation of Versions 5.0.1, 5.1.0, and 5.2.0, NASA Technical Report Series on Global Modeling and Data Assimilation, V27.

Rodell, M., J.S. Famiglietti, and B.R. Scanlon, 2010: "Realizing the Potential of GRACE for Hydrology", EOS Trans. AGU, 91 (10), p. 96.

Rodell, M., P. R. Houser, A. A. Berg, J. S. Famiglietti, 2005: Evaluation of 10 Methods for Initializing a Land Surface Model. *J. Hydrometeor*, **6**, 146–155. doi: http://dx.doi.org/10.1175/JHM414.1

Saji, N. H., B. N. Goswami, P. N. Vinayachandran, & T. Yamagata, 1999: A dipole mode in the tropical Indian Ocean. Nature, 401, 360–363.

Schmugge, T.J., (1985). Remote Sensing of Soil Moisture. In: Hydrological Forecasting. M.G. Anderson and T.P. Burt, eds. John Wiley, New York.

Sellers, P.J., Y. Mintz, Y.C. Sud, and A. Dalcher, 1986: A simple biosphere model (SiB) for use within general circulation models. J. Atmos. Sci., 43, 505-531, doi: http://dx.doi.org/10.1175/1520-0469(1986)043<0505:ASBMFU>2.0.CO;2.

Stieglitz, M., A. Ducharne, R.D. Koster, and M.J. Suarez, 2001: The impact of detailed snow physics on the simulation of snow cover and subsurface thermodynamics at continental scales. J. Hydromet., 2, 228-242, doi: http://dx.doi.org/10.1175/1520-0469(1986)043<0505:ASBMFU>2.0.CO;2.

Tapley, B. D., S. Bettadpur, J. C. Ries, P. F. Thompson, and M. M. Watkins, 2004: GRACE measurements of mass variability in the Earth system, Science, 305, 503-505, doi: 10.1126/science.1099192.

Wang, J.R., and T.J. Schmugge, (1980). "An empirical model for the complex dielectric permittivity of soil as a function of water content", *IEEE Trans. Geosci. Remote Sensing*, **18**:288-295.

Yatheendradas, S., Christa D. Peters Lidard, Victor Koren, Brian A. Cosgrove, Luis G. G. De Goncalves, Michael Smith, Jim Geiger, Zhengtao Cui, Jordan Borak, Sujay V. Kumar, David L. Toll, George Riggs, Naoki Mizukami, 2012: Distributed assimilation of satellite-based snow extent for improving simulated streamflow in mountainous, dense forests: An example over the DMIP2 western basins, Water Resour. Res., 48, W09557, doi:10.1029/2011WR011347.

Zaitchik, B.F., M. Rodell, and R.H. Reichle, 2008: Assimilation of GRACE terrestrial water storage data into a land surface model: results for the Mississippi River Basin, J. Hydrometeor., 9 (3), 535-548, doi:10.1175/2007JHM951.1.